New horizons in structure-function studies of copper nitrite reductase

Robert R. Eady, S. Samar Hasnain

Molecular Biophysics Group, Department of Biochemistry and System Biology, Institute of System, Molecular and Integrative Biology, Faculty of Health and Life Sciences, University of Liverpool, Liverpool, L69 7ZB, United Kingdom.

Abstract

In recent years there have been paradigm shifts in our understanding of the diversity of copper-containing nitrite reductases (CuNiRs) found in nature, as genomic mining revealed the extent of the distribution of variants with additional tethered redox domains. The availability of these variants is an unparalled opportunity to explore inter-protein electron transfer events that are so important in biology. Access to X-ray free-electron laser sources with femtosecond X-ray pulses has enabled crystal structures of several CuNiRs to be determined free of radiation-induced damage and radiation-induced redox chemistry. By controlling the radiation dose, structural movies of enzyme-bound intermediates of the catalytic cycle have been identified, notably the relevance of a Cu-NO species to catalysis has been established. Such studies have been complemented by an approach using chemically induced turnover of enzyme in crystals. These have allowed damage-free high-resolution, even atomic resolution, structures to be analysed to assign probable protonation states of critical residues complemented by ambient temperature and our neutron crystallographic structure. The determination of X-ray crystal structures at elevated temperatures including room temperature revealed a stable Cu-nitrosyl intermediate during in-crystal turnover. This should enable refinement in computational chemistry modelling and enable a more rational comparison with spectroscopic data relating to solution studies. Using advanced biophysical techniques the link between proton uptake and inter-Cu electron transfer been established. Spectroscopic single-molecule studies have revealed differences in redox behaviour of isolated enzyme compared with turnover. These are significant advances that together with recent refinement of computational models of the CuNiR reaction mechanism are likely to assist in the development of synthetic CuNiRs.

1 Introduction

Copper-containing nitrite reductases, (CuNiR; EC 1.7.99.3) encoded by *nirK,*) are a highly conserved family of enzymes, widely distributed in nature and found in all three kingdoms of life. They catalyse the reduction of nitrite to nitric oxide

$NO_2^- + e^- + 2H^+ \leftrightarrows NO + H_2O \quad E'_{o\ (pH\ 7.0)} + 370mV$ Eqn. 1

and are involved in several microbial energy-generating pathways in which O_2 is not the terminal electron acceptor. These processes are major players of the global biogeochemical nitrogen cycle. The role of CuNiR in denitrification is widely recognised [1] but less appreciated is their involvement in nitrification [2], the aerobic conversion of NH_3 to nitrite, and to a lesser extent in anammox [3], the anaerobic oxidation of NH_3 to N_2 using nitrite as electron acceptor. These metabolic activities of organisms result in the emission of N_2O from soils and ocean waters into the atmosphere, with a strong negative environmental impact [4]. Although N_2O is a trace atmospheric gas, it has a global warming potential ~300-fold higher than CO_2 and its concentration is increasing. As a consequence, study of the sources of N_2O and its ocean-atmosphere flux has been subject of intense study. CuNiRs are relevant to these broad issues since they produce NO, the substrate for nitric oxide reductase, which is the major biological source of N_2O. CuNiR also has an important medical role in enabling pathogens such as *Neisseria* species, the causative agents of meningitis and gonorrhoea, and the opportunistic pathogen *Alcaligenes xylosoxidans* to survive in oxygen-limited tissues using denitrification to generate ATP [5,6]. The NO and superoxide released in the host immune response on infection is neutralised by the reversibility and superoxide dismutase activities of CuNiR. In addition quinole-dependent nitric oxide reductases that are commonly found in pathogenic bacteria provide an additional means of evading the host response [7]. From a chemical viewpoint CuNiRs have generated interest because of the unusual binding mode of nitrite and NO to the active site Cu seen in crystal structures that do not have precedence and as such represent new Chemistry. These studies have catalysed significant biomimetic efforts in an attempt to provide synthetically produced CuNiRs that are able to deliver NO for biomedical applications [8]. In this review we focus on recent advances in the detail of substrate binding, inter-Cu ET, proton uptake and catalysis informed by cutting-edge crystallographic and advanced biophysical techniques as applied to prototypic CuNiRs. In addition, the domain-extended CuNiRs that present a challenge to understanding inter-domain ET, and the moderation of catalytic activity of the core enzymes are reviewed.

2. Overview of prototypic CuNiRs and the more recently identified domain-extended variants

Copper coordination of redox and catalytic centres in biology is extremely diverse but the protein environment has a common domain structure. The cupredoxin fold, a building block widely used by Nature to construct proteins involved in respiration, photosynthesis and denitrification, has an eight β-strand beta-barrel, often duplicated within a protein domain, The most widely-studied CuNiRs are those originating from a number of denitrifying organisms [reviewed in [9,10,11] but representatives from nitrifying [12] and anammox organisms [13] have also been characterised, (Fig 1).

INSERT Figure 1 here.

Numerous crystallographic studies of these enzymes, subsequently referred to as prototypic NiRs, retain the same core structure and active site features despite having amino acid sequence identity as low as 30% [11]. The enzymes from denitrifying and nitrifying organisms are trimeric and each monomer is made up of a duplicated cupredoxin fold harbouring a single type-1 Cu site (T1Cu) and a catalytic type-2 Cu site

(T2Cu) located at the interface of adjacent subunits. There is a single recently identified and structurally-characterized hexameric variant of this theme, isolated from the anammox bacterium KSU-1 [13]. The hexamer is stabilised by disulphide bond formation between trimers, a feature not seen in other CuNiRs. This form of a CuNiR may have a wider distribution since a preliminary report indicated the enzyme from a denitrifying archaeon was also hexameric [14].

The increase in the number of available genome sequences has enabled data mining to identify domain variants of *nirK* and several extended CuNiRs have subsequently been biochemically and structurally characterized, (Fig 2). These variants with cupredoxin or heme extensions are widespread among α, β and γ-proteobacteria. Geneomic analysis revealed that ~30% of *nir*K-dependent denitrifiers [15] have extended CuNiRs with additional C- or N- terminal domains, with C-terminal extension being more common, suggesting that these variant enzymes play an important role in the nitrogen cycle, Figure 2. In addition, ~ 5% of NirK denitrifyers were shown to have more than one *nirK* gene copy [15].

INSERT Figure 2 here

The most recent addition to the multi-domain Cu-NiR family identified in several members of the order *Rhizobiales* [16] is a 4-domain enzyme (4D-CuNiR) with both heme and cupredoxin N–terminal extensions. All organisms with this new variant have an additional copy of *nirK* encoding a 2D-CuNiR. To date there is no information as to the functionality of additional copy of *nirK* genes. It has been speculated that their expression is linked to different environmental conditions of aerobiosis or nitrite availability or have a role other than the reduction of nitrite. Likewise, our understanding of the functional advantages of C- or N-terminal tethering with putative electron donor domains is at an early stage, requiring significant multi-disciplinary effort. Another aspect of the catalytic potential that has not been widely recognised and studied is that many CuNiRs also have a weak oxidase activity and catalyse the two-electron reduction of dioxygen to H_2O_2, a product that in the absence of catalase inactivates prototypic CuNiRs [17]. The nitrifying organism *Nitrosomonas europaea* has a membrane-associated CuNiR that is active under aerobic conditions. Characterisation of this enzyme showed it does not reduce dioxygen and the crystal structure revealed a more restricted access channel to the active site compared to prototypic CuNiRs [12].

In addition to the reaction with dioxygen, CuNiRs also catalyse the two electron reductive coupling of NO to form N_2O when exposed to excess NO [18]. This reaction has led to the re-evaluation of the spectroscopic data for NO binding to as-isolated CuNiR (see section 7.1). *In vivo* studies have shown the involvement of *nirK* in the reduction of toxic selenite to elemental selenium by the non-denitrifying organism *Rhizobium sullae* tolerant of [mM] selenite concentrations [19].

3. Global structure and overview of catalysis in prototypic CuNiRs

The widely-studied prototypic CuNiRs are homotrimers with each subunit containing a T1Cu centre with Cys-Met-$(His)_2$ ligation that receives electrons from physiological electron donors, the periplasmic redox proteins cupredoxins, azurins or pseudoazurins,

or *c*-type cytochromes in different organisms. The colour of CuNiRs from different sources as isolated varies, being blue, bluish-green or green, arising from the oxidized T1Cu site. Typically the absorption spectra of the blue enzymes is dominated by broad features at ~590 nm and have an axial EPR spectrum and the green enzymes by bands at ~460 and ~600 nm and rhombic EPR features. Atomic resolution crystal structures of blue and green CuNiRs show that the colour correlates with the length of the weak Cu-Met bond and small differences in coordination geometry. The blue and green enzymes have markedly different surface charges. The catalytic T2Cu centres are located at the interface of two adjacent subunits and have tetrahedral geometry usually with $(His)_3$-H_2O ligation with one His residue provided from an adjacent monomer and is accessed from the bulk solvent some 12 Å away by a ~6 Å wide channel between monomers. The T2Cu is linked to the electron-donating T1Cu centre *via* a Cys-His bridge resulting in a Cu-Cu separation of ~12.6 Å, Figure 3. A second longer four-residue bridge connects His ligands of T1 and T2Cu sites and harbours an Asp residue (termed Asp_{CAT}) that forms a H-bond with the T2Cu H_2O ligand of the resting enzyme and with bound nitrite when it displaces the H_2O ligand, and also to the product NO. This link has a proposed sensor role and communicates the binding of substrate at the T2Cu to the T1 Cu site resulting in a rapid transfer of electron required for the reduction of nitrite (Fig 3). There is a body of spectroscopic data indicating that the binding of nitrite to the catalytic T2Cu results in changes to the T1Cu. A resonance Raman study of *Ax*NiR showed the υ(Cu-S_{Cys}) bands at 412, 420, and 364 cm^{-1} all shifted to higher frequencies when nitrite bound consistent with efficient communication between the two Cu sites [20]. Additional evidence for cross-talk between the oxidized Cu centres in the absence of nitrite, is provided by EPR data for His154Ala and Met150Glu substitutions of the T1Cu ligands of *Af*NIR which show altered T2Cu parameters compared with WT enzyme [21, 22]. This interaction is independent of the oxidation state of the T1Cu since these changes are observed in T1Cu H139A H145A substituted *Ax*NiR and *Af*NiR respectively [23, 24] where due to the elevation of the reduction potential to 7-800 mV the T1Cu of the isolated enzyme is reduced.

INSERT Figure 3 here

Two invariant active site pocket residues Asp_{CAT} and His_{CAT} are involved in substrate-binding and effective catalysis are linked by H-bonds to a bridging H_2O molecule. A conserved Ile_{CAT} residue ~3 Å from the bound substrate caps the active site pocket to provide steric control of ligand access to the T2Cu. Molecular dynamics simulations of *Ax*NiR show that the protonation states of Asp_{CAT} and His_{CAT} strongly influence the solvent accessibility of the active site [25]. Two potential proton channels from the T2Cu to the protein surface have been identified in *Ax*NiR, [26] but are not present in all CuNiRs. In *Ax*NiR where proton uptake has been studied, mutagenesis has established the predominant route. In different enzymes there is also some variation in the surface loops, the 'linker' loop connecting the two cupredoxin domains of the monomer, and the 'tower loop' positioned above the T1Cu site and important in interaction with electron donor proteins. When proton uptake is compromised as in the N90S variant, crystallographic studies showed that in nitrite-bound *Ax*NiR a significant movement in the loop connecting the T1 Cu ligands Cys130 and His139 closed the substrate binding pocket and exposed the T1Cu site to potential electron donor proteins azurin or cyt *c* [27]. The binding of nitrite to the T2Cu of CuNiRs as-isolated, displaces the H_2O ligand and crystal structures show it to bind via both oxygen atoms irrespective of the organism

[11, 28]. The product NO binds in an unusual side-on mode to the T2Cu when generated by enzyme turnover in crystals using either electrons generated by X-rays, or treatment of nitrite-soaked crystals with a chemical reductant, or when NO is diffused into crystals [29, 30, 31, 32, 33], (Fig 4).

INSERT Figure 4 here

During steady-state turnover the consensus view is that a 'random sequential mechanism' operates in which the order of nitrite binding and reduction of the T1Cu is dependent on [nitrite] and pH. This mechanism was proposed based on detailed kinetic study of *Af*NiR using pseudoazurin, viologens or protein-film voltammetry methods as a source of electrons [34]. Combined fluorescence and electrochemical measurements of the oxidation state of the T1Cu of *Af*NiR during turnover were consistent with this scheme. A spectro-electrochemical approach was used to control the redox state and turnover electrochemically, and determine the T1Cu oxidation state from fluorescence changes [35]. The [nitrite] and pH-dependence of activity of labelled *Af*NiR absorbed on a modified gold electrode was determined over the pH range of 5.45 and pH 6.85, essentially straddling the pH activity dependence curve. At the lower pH the sequential addition of nitrite progressively oxidized the T1Cu and increased the catalytic current until ~ 520 μM nitrite, subsequently activity decreased, and the T1Cu became progressively more oxidised as [nitrite] was increased. At the higher pH similar stepwise response to increasing [nitrite] was observed but substrate inhibition did not occur up to 27.5 mM. The data were a good fit to the random sequential model where at low [nitrite] reduction of the T2Cu occurs before nitrite binds (route A) and at high [nitrite] shifts to route B where reduction of the nitrite-bound T2Cu is predominant. At pH 5.45 the T2Cu is predominantly reduced before nitrite binds but as [nitrite] is increased, binding occurs first shifting from route A to B resulting in a ~100-fold decrease in the fit for the inter-Cu ET rate. This decrease is seen in single-turnover pulse radiolysis and laser-flash photolysis experiments where the electron is transferred to a pre-formed $T2Cu^{++}$-nitrite species (see section 5.3). These studies on an immobilised green CuNiR have been extended to solution studies of single molecules of the blue *Ax*NiR where the kinetic parameters during turnover indicated both routes operated dependent on [nitrite] [36]. The operation of two parallel ordered pathways with markedly different rates of inter-Cu ET, proton uptake and enzyme activity dependent on [nitrite] and pH, provide further support for its operation in prototypic CuNiRs. In contrast, the N-terminal cupredoxin extended 3D-NIR, *Hd*NiR and the N-terminal heme extended *Ph*NiR inter-Cu ET only occurs in the presence of nitrite restricting them to the 'nitrite-binding before reduction' route.

Crystallographic and electron nuclear double resonance studies (ENDOR) have shown nitrite binds to the oxidized T2Cu by displacement of the H_2O ligand. If the T2Cu is reduced in the absence of nitrite the H_2O ligand dissociates and the enzyme is inactivated [37, 38] and the $(His)_3Cu^+$) site is unable to bind nitrite or the inhibitor azide. A careful study of ascorbate reduced *Ac*NiR utilising single shot diffraction of X-ray laser pulses on 33 large crystals has provided a detailed picture of the T1Cu and T2Cu site in response to chemical reduction [39]. Water is lost from the T2Cu site producing a tricoordinate T2Cu site with three histidine residues ligating the copper in a manner similar to reduced superoxide dismutase Cu site [40]. The T2Cu also drops 0.5 Å into the histidine plane upon reduction. The electron density of the side chain of $Ile_{CAT}257$

revealed that the CD1 side chain flips down to partially occupy the space vacated by the water ligand, reducing the volume and increasing the steric restraints on the active-site cavity.

When nitrite is used to initiate steady-state turnover of reduced enzyme the activity is lower than when turnover is initiated by adding enzyme. This indicates that nitrite can productively bind to the $H_2O(His)_3Cu^+$) site. The lower activity presumably arises from a balance of the rate of dissociation of water from the reduced T2Cu site to form the inactive tri-coordinate Cu site and the time before nitrite is added to the assay.

Experimentally, the 'nitrite-binding before reduction' route is most accessible in the study of catalysis since the provision of electrons to initiate reaction is more easily controlled. As a consequence, measurements of inter-Cu ET, rates of proton uptake, and structural movies of catalysis all focus on events in a single turnover starting from the enzyme with $T1Cu^{++}$-$T2Cu^{++}$ with or without nitrite bound. An exception is the studies of the control of proton delivery in pH perturbation experiments where $T1Cu^{+}$-$T2Cu^{++}$-nitrite is the starting species for the measurement of ET and proton uptake (see section 5.5).

'The reduction first' route is not easily studied in the same way since the shift from the $T1Cu^{++}$-$T2Cu^{++}$ state to the $T1Cu^{+}$-$T2Cu^{+}$ starting point is spectroscopically silent and coupled proton uptake and inter-Cu ET has already occurred.

4. Modes of nitrite and NO binding to resting enzyme

Early crystallographic studies showed nitrite-soaked crystals of as-isolated *Ac*NiR bound nitrite in bidentate η^2-O,O mode to the T2Cu [28]. In the following quarter of a century many other structures have been determined and show the same binding mode but with some variation in geometry [see 9,11]. The first crystal structure of NO-bound CuNiR reported 17 years ago was observed in ascorbate-reduced crystals of *Af*NiR soaked with excess NO under anaerobic conditions [29]. The side-on binding mode of NO to the T2Cu was unprecedented but has been confirmed in all subsequent crystal structures either from NO soaking of crystals, intrinsically bound, or generated from the reduction of nitrite in turnover in crystals using a chemical reductant or electrons generated from X-ray radiolysis [31, 32, 41]. The unusual mode of binding of both nitrite and NO has attracted considerable interest in the computational chemistry and biomimetic chemistry communities.

4.1 Binding of nitrite

Some of the variation in the binding geometry of nitrite in CuNiR structures is likely to have arisen due to partial reduction of the T2Cu during the synchrotron data collection, where X-rays used to collect data result in significant level of radiolysis creating an internal electron source (See Section 6). This is exemplified by comparison of the SR X-rays (SRX) and X-ray Free Electron Laser (XFEL) structures free from radiation-induced chemistry (FRIC) of Br^{2D}NiR [32]. The XFEL-FRIC structure (1.3Å) of nitrite-bound enzyme showed a single, previously unobserved side-on conformation of nitrite with all three atoms at very similar distances to the T2Cu of 2.12, 2.02 and 1.92 Å. Single crystal spectroscopy clearly showed that T1Cu is in the Cu^{2+} state while observing a well-defined LMCT charge transfer band at ~360 nm from nitrite to T2Cu, (Fig 5). This is the first time that this spectral signature of nitrite has been observed, which is difficult to observe in solution due to overlapping absorption of free nitrite in solution. We note that very limited spectroscopic work (EPR, ENDOR, optical) has been done on single

crystals of CuNiRs. The SRX structure of nitrite bound Br^{2D}NiR (1Å) showed full occupancy of nitrite bound to T2Cu in a bidentate η^2-O, O mode in two alternative 'top-hat' conformations. The very high resolution of 1 Å for this structure allowed SHELX unconstrained refinement that showed one orientation with Cu-O distances of 2.13(6) Å and 1.98(2) Å, the second 'bent top-hat' had slightly longer distances of 2.22(5) Å and 2.13(2) Å. The nitrite is H-bonded to Asp_{CAT} in two conformations, a proximal position as seen in as-isolated Br^{2D}NiR and a gatekeeper position first reported for non-recombinant green *Ac*NiR 0.89 Å) [41]. The occupancies of (0.6) and (0.4) for the proximal and gatekeeper positions correlate well with the 'bent top-hat' and 'top-hat' orientations of nitrite. Analysis of carboxyl bond lengths was consistent with them being unprotonated in both conformations. His_{CAT} C-N-C bond angles corresponded to full protonation, in contrast to the as isolated enzyme.

INSERT Figure 5 here

The assignment of the protonation states of Asp_{CAT} and His_{CAT} are in agreement with spectroscopic and DFT modelling of nitrite-bound *Rs*NiR with reduced T1Cu [42]. There is a single incidence of η^2-O binding in *Gt*NiR at 100 K that reverted to the η^2-O,O mode at RT in the C134A variant where photolytic ET was compromised [43]. In this CuNiR, Ile_{CAT} is replaced by $Val_{CAT,}$ a smaller residue providing more space in the catalytic pocket. The Ile to Val_{CAT} is a natural variant seen in very few CuNiRs, only two, *Gt*NiR and the recently isolated three-domain *Ts*NiR [44] have been structurally characterised. The importance of Ile_{CAT} as a key determinant in controlling the productive mode of nitrite binding was shown from the properties of six structurally characterised variants of *Af*NiR [45]. When monodentate binding was observed, activity was significantly lowered to ~ 1-4% of WT and the bound nitrite no longer formed a H-bond with Asp_{CAT}. The Ile_{CAT} to V/L variants showed bidentate η^2-O, O binding and had 124% and 25% activity respectively compared with WT.

Solution studies of nitrite binding to *Rs*NiR have utilised changes in the ENDOR spectra induced by nitrite binding [46] or the depletion of the FTIR 1237 cm^{-1} band of free nitrite or the N—O stretching vibration of bound nitrite 1386 cm^{-1} [47]. The pH dependence of nitrite binding showed a pKa of 7.4 for half maximal binding. The EPR spectra of nitrite-bound *Rs*NiR show a pH interconversion of two species with a pKa of 6.4 [42]. DFT calculations for pH 8.4 where inter-Cu ET does not occur due to a decrease in the reduction potential of the T2 site, the best fit for the protonation states were deprotonated Asp_{CAT} and protonated His_{CAT} in the $T1Cu^{+}T2Cu^{++}$-nitrite species. The pH dependent changes of the EPR spectra were attributed to protonation of Asp_{CAT}. The significance of these binding modes and protonation states to enzyme turnover is discussed in sections 5.5 and 6.1.

4.2 Binding of NO

On prolonged exposure of crystals to excess NO, as-isolated oxidised *Af*NiR catalyses the reverse reaction and a well-ordered nitrite was observed bound to the T2Cu and H-bonded to Asp_{CAT} [30]. When inter-Cu ET is disrupted, as in the T1Cu mutant H145A where the reduction potential is raised to ~800mV, exposure of crystals to excess NO resulted in side-on binding being observed with Cu—N and Cu—O bond distances of

2.09 and 1.99Å respectively. In summary, crystallographic data support the formation of a side-on Cu-nitrosyl when oxidised or reduced *Af*NiR is exposed to excess NO provided the reverse reaction to form nitrite is impaired (see section 6).

EPR spectra (80 K) of *Af*NiR-NO complexes were assigned to side-on Cu^{++}-NO^{-} adducts [30]. However, this has subsequently been challenged since EPR, MCD and ENDOR studies of the reaction of reduced *Rs*NiR with excess NO indicated the product as $T1Cu^{+}$-$T2Cu^{++}$-nitrite [48]. Only in the presence of limiting [NO] was a Cu-nitrosyl species $T1Cu^{+}T2Cu^{+}NO^{\cdot}$ formed by *Rs*NiR. Analysis of EPR data was consistent with end-on binding with a ~160^{o} Cu-N-O angle, and the H^{1} coupling features in the ENDOR spectra, an interaction with $Ile_{CAT.}$

5. Inter-Cu electron transfer in the absence of nitrite

Many studies of CuNiRs have shown that the driving force for ET, the positive difference between the reduction potential of T1 and T2 copper centres, is very small and in some cases energetically unfavourable in the absence of substrate. *Pc*NiR represents the extreme example of this among prototypic CuNiRs with reduction potentials of T1Cu +298 mV and T2Cu +172 mV at pH 7.6 [49] a difference in potential that EPR measurements show allows selective reduction of the T1Cu by ascorbate/or NADH/PMS as reductant. The physiological route for electron input leading to the reduction of the Cu centres is via the T1Cu site positioned close to the enzyme surface and with a solvent exposed $N\varepsilon_2$ atom of a His ligand. This has been shown to be the primary route for the artificial donors dithionite [50] and photo-electrons generated by exposure to high X-ray doses in synchrotron radiation experiments [51].

There are differences in the details of the electron transfer routes between the two copper centres of blue and green NiRs. In blue CuNiRs there is a direct interconnecting bridge through the protein backbone involving the S(Cys) carbonyl group of the T1Cu to the His-$N^{\delta 1}$ ligand of the T2Cu. Green CuNiRs have an additional pathway through the S(Cys) amide H—bonded to the His T2Cu. DFT calculations indicate that the high covalency of the T1Cu-S(Cys) bond results in electronic coupling that facilitates long-range ET through both pathways with the H—bonded path possessing a higher overall efficiency [52].

5.1 Solution studies of inter-Cu electron transfer

The transient changes in the strong charge-transfer band of the Cu^{++}-Cys of the oxidised T1Cu have been widely applied in studies of the kinetics of ET in solution. Both pulse radiolysis and laser-flash photolysis of CuNiRs result in an electron rapidly reducing the T1Cu on a timescale faster than conformational changes can occur. In both of these probes a substantial pool of electrons is generated. Subsequently, thermodynamic equilibrium is re-established by ET from the reduced T1Cu to the oxidized T2Cu centre enabling both the rate of ET and the thermodynamic redox equilibrium to be determined. The equilibrium position is determined by the difference in mid-point reduction potential of the T1and T2Cu centres. The rate of ET is determined by this difference, the distance between the Cu centres, the electronic pathway and the reorganizational energy. Studies of prototypic CuNiRs are restricted to *Ac*NiR, *Ax*NiR and several mutant variants of residues in the catalytic pocket [for review see 53]. The reduction potentials of T1Cu

and T2Cu of *Ax*NiR are +255 and +244 mV and for *Ac*NiR +240 and +250 respectively providing only a small driving force for reduction of the T2Cu. The potential of the T1Cu is pH independent, but pulse radiolysis and laser-flash photolysis studies show that the potential of the T2Cu is pH-dependent. For both *Ac*NiR and *Ax*NiR the pH dependence of the difference in reduction potential between the two Cu sites showed redox-coupled proton dissociation constants for $T2Cu^{++}/Cu^{+}$ with pK_{ox} ~ 5 and pK_{red} ~ 7 [54]. The temperature dependence of the rate of ET enabled determination of the activation parameters for ET [55]. The green *Ac*NiR had a higher ET rate of 1030 s^{-1} compared to blue *Ax*NiR 450 s^{-1} despite a lower driving force and was attributed to differences in the total reorganisation energies of 1.16 and 1.26 eV respectively. The T2Cu site reorganizational energy was markedly higher than that of the T1Cu site and was rationalised in terms of solvent accessibility and H-bonding networks. The activation entropy of green *Ac*NiR was also higher, consistent with electron tunnelling being slightly more advantageous possibly due to the geometry of the electron transfer routes between the two copper centres of blue and green NiRs (see Section 5).

More recently a ^{60}Co-source of γ-radiation has been utilized to cryolytically reduce *Ax*NiR and assess the extent of ET at pH 7 and 80k by EPR spectroscopy [56]. Partial reduction (30%) of the T1Cu did not result in any detectable ET to the T2Cu site similar to the observations in T1Cu reduced crystals [51]. This behaviour was attributed to a requirement for thermally-driven protein motions for PCET to occur. The direct involvement of protons in the ET reaction in the absence of nitrite was evident in laser-flash photolysis single-turnover studies of *Ax*NiR in D_2O where a SKIE of 1.3 was observed indicating that inter-Cu ET is linked to a proton transfer step irrespective of catalysis [57] possibly involving Asp_{CAT} and His_{CAT} being linked to PCET in CuNiR [58].

5.2 Inter-Cu electron transfer in crystals

There is a clear difference between solution ET studies and reactivity in crystals of *Ax*NiR since the redox equilibrium of the Cu centres described above is not observed. A combination of x-ray crystallography and on-line spectroscopy showed that photo-electrons generated by exposure to high X-ray doses (1.5 x10^6 Gy) selectively and rapidly reduced the T1Cu [51, 59]. The T2Cu, in contrast, clearly remained in the Cu^{2+} oxidation state as confirmed by the XANES spectroscopy of a single crystal collected after two complete data sets for X-ray crystallographic structures, Figure 6. The XANES spectrum showed the shoulder associated with Cu^{2+} but with a small shift in the edge to lower energy, consistent with T1Cu being reduced as indicated by bleaching of of 590 nm band in the optical spectrum. Thus, the redox equilibrium of the Cu centres seen in solution at RT is not apparent in crystals at 100K. This situation changes when nitrite is diffused into crystals of both blue and green NiRs subsequent exposure to X-rays induces inter-Cu ET and reduction of nitrite resulting in the formation of a Cu-NO species. (see Section 6.3.1). We note that XANES reports on both distances and geometry of ligands in the coordination sphere at very high resolution and that the solution XANES spectrum and that of enzyme crystals were identical, confirming the equivalence of copper sites in solution and crystals.

INSERT Figure 6 here

5.3 Inter-Cu electron transfer in the presence of nitrite

The energy barrier for ET presented by the small difference in redox potentials of the Cu centres is overcome in the presence of substrate, and the consensus view is that this is due to a significant rise in the mid-point reduction potential of the $T2Cu^{++}$ centre on nitrite binding [see 9]. In both pulse radiolysis and laser-flash photolysis studies the presence of nitrite alters the rate of ET as the enzyme undergoes a single turnover of a $T2Cu^{++}$-nitrite starting species. Depending on the pH, the rate of ET is the same (pH 6) or is strongly inhibited (pH7.5) [60]. Both *Ac*NiR and *Ax*NiR exhibited an ET rate with a bell-shaped pH dependence over the range 5 to 7.5 with a maximum ~ pH 6 the optimum pH for activity (Figure 7). In the presence of nitrite, this pH dependence behaviour is essentially the same as that observed for the apparent catalytic rate constant [60] suggestive of ET being the rate-limiting step in enzyme turnover. A similar pH dependence of activity of *Rs*NiR at pH7.2 was observed using the electron donor iso-1-*cytc* (E_o +273 mV). Substitution of T1Cu(Met182Thr) elevated the reduction potential by 100 mV and perturbed the activation energy for activity over the pH range 5-7.5 confirming ET from T1Cu to nitrite-boundT2Cu is rate-limiting under these conditions [46].

INSERT Figure 7 here

However, the [nitrite] dependencies of steady-state activity and the rate of ET of *Ax*NiR at pH 7 are different, indicating that the inter-Cu ET step in this case cannot be rate-limiting [27]. As described below, the requirement for proton uptake as a step prior to ET and the kinetic coupling between them [57] makes proton transfer the likely rate-limiting step in turnover in *Ax*NiR. This is consistent with the finding that subtle changes in proton delivery resulting from directed mutations affecting solvent accessibility have been shown to change the rate-limiting step. For example, when the main proton channel of *Ax*NiR, the highly ordered H-bonded water network (Asp92**-**water-water**-**Ala131**-**Asn90**-**Asn107) from the T2Cu site to the bulk solvent [26] is disrupted by the N90S substitution, the activity is decreased, but in contrast to WT enzyme similar patterns of the [nitrite] dependence of the rate of ET and steady-state activity are observed [27]. This correlation was also an effect of substitution of a surface residue (F306C) some 12 Å from the T2Cu centre of *Ax*NiR, this opened up the substrate access channel and an altered H_2O network at the active site resulting in a change of rate-limiting step [61].

The ability of nitrite to trigger inter-Cu ET in crystals over a wide temperature range including ambient temperature finds a clear explanation in that changes in ligand field associated with the displacement of water by nitrite increases the reduction potential of the T2Cu and alters the reorganizational energy to favour an effective ET. It is evident from the X-ray structural movies using MSOX (Multiple Structures from One Crystal) serial crystallography that once catalysis is initiated the mobility of critical residues of the active site pocket Asp_{CAT} His_{CAT} and Ile_{CAT} are not constrained by the crystalline environment of the enzyme molecules.

There are also spectroscopic and computational data suggestive of the cryo-temperature dependence of the T1Cu site in green NiRs [62]. Comparison of the T1Cu sites of blue and green NiRs with those of the blue centres of azurin/pseudoazurin and multi-copper oxidases, show that the Sδ-Met-Cu bond lengths in CuNiR are shorter

(~2.6Å compared with ~ 2.8 to 3.2Å [63]. Resonance Raman spectroscopy and DFT calculations for *Rs*NiR have suggested a thermodynamic equilibrium of two T1Cu species $[Cu\text{-}Met]_{green} \leftrightarrows [Cu]_{blue}$ + Met. However, XFEL-FRIC high resolution (1.3-1.6Å) structures of *Ax*NiR (blue), *Br*2DNiR (greenish blue) and *Ac*NiR (green) have all revealed Cu-S_{Met} distances in the range of 2.6-2.7Å with a similar distance seen in the *Ac*NiR structure obtained from neutron diffraction data collected at room temperature. These data do not support the suggestion that the difference in absorption spectra at ambient temperature may arise from a lack of constraint for the Met ligand, whose dissociation at room temperature being reflected in the absorption spectra [62]. This is also consistent with an ENDOR study of WT*Rs*NiR and the M128T variant. This substitution raised the redox potential and resulted in a green to blue colour change, but the critical HOMO were unaltered at the His/Cys residues. The authors concluded that subtle protein conformational differences rather than different methionine ligation was responsible [64].

5.4 Single molecule solution studies of Inter-Cu electron transfer

Single-molecule fluorescence lifetime imaging revealed two populations of molecules during turnover corresponding to two distinct mechanisms for the conversion of nitrite to NO. The predominant route depends on [nitrite]. At low [nitrite] the majority of the molecules undergo ‘reduction before binding’ and increasing [nitrite] shifts to ‘binding before reduction’ [see 65 for review].

The combination of laser excitation and confocal microscopy to study single molecules labelled with a fluorescent dye allows the oxidation state of the T1Cu during turnover to be determined. Initial studies used *Af*NiR modified by attachment of a fluorophore close to the electron entry site, and immobilised through a linker onto salinized glass coverslip [66]. Under conditions favouring ‘reduction before binding’ and ascorbate/PES as reductant Förster, resonance energy transfer from the charge transfer band of the oxidized T1Cu and the fluorophore allowed the oxidation state of the T1Cu during turnover to be determined from fluctuations in fluorescence intensity. Data were consistent with enzyme turnover but individual turnovers could not be resolved We note that it is not known if the attachment of dye to *Af*NiR effects the structure of NiR in any way particularly the catalytic core, although the activity and apparent K_M for nitrite were not perturbed in bulk solution measurements.

A later study of untethered labelled *Ax*NiR enabled fluorescent decay times to be determined for oxidised and reduced enzyme [67]. Under turnover conditions two distinct populations, one with 20-30 ms and a second with 10 ms for a T1Cuox/red transition were observed, with the ratio dependent on [nitrite] over the range 5μM to 5 mM. To obtain prolonged data collection over several seconds for single molecules in a solution-phase environment rather than tethered or gel-entrapped molecules, a micro-fluidic trapping technique, the anti-Brownian electrokinetic ABEL trap was used. Using this technique provided better time resolution and turnover of trapped *Ax*NiR molecules could be followed for several sec and the distribution between oxidized and reduced levels measured. The dual-time distribution between the two states enabled kinetic data to be extracted and an ET scheme proposed. Two populations of molecules were observed, one with T1Cu remaining reduced most of the time and a second switching between reduced and oxidised states. The ratio between the two populations was dependent on [nitrite], consistent with a random-sequential mechanism operating [34]. A surprising finding from this study was the stochastic nature of events in which a given

molecule remains in one branch of the pathway e.g. reduction-before-binding for several minutes before switching to the 'binding-before-reduction' pathway.

The difference in the pattern of [nitrite] dependence (see section 3) appears to allow the assignment of which route is functioning. However, while the focus of this scheme has been on the [nitrite] on the redox balance of the Cu centres, the PCET dependence of inter-Cu ET results in pH also determining which of the two routes is operative [68]. In these alternative routes, each of them follows a clear order of reaction and as such, a better description of the mechanism would be 'alternate-route ordered mechanism'. In this case, the microscopic reversibility of the well-defined 'binding before reduction' route would not be applicable to both, and the 'reduction before binding' may utilise the predominantly computationally favoured N-binding of nitrite and the formation of a T2Cu-OH resting state. Under conditions where both operate, the transition of a single molecule between routes may account for the two distinct populations observed [67].

5.5 Proton uptake associated with Inter-Cu electron transfer

Proton-uptake inventory measurements of *Ax*NiR in multiple turnover experiments showed the involvement of two protons per nitrite reduced consistent with structural studies where H_2O not OH^- is displaced from the resting enzyme when nitrite binds [57]. In D_2O a solvent kinetic isotope effect (SKIE) was observed in steady-state experiments consistent with the involvement of a protonation event in the rate-limiting step in turnover at pH 7. These findings contrast with the finding for *Rs*NiR at pH 6 where no SKIE was observed [46] suggesting that the rate-limiting step in ET is no longer proton coupled. However, the lack of a SKIE was apparent from measurements of the rate of oxidation of iso-1ferrocyt *c* used as an electron donor where proton transfer must occur before or after the rate-limiting step, identified as the T1 to T2 ET reaction.

In order to gain insight to the involvement of protons in AxNiR, laser-flash photolysis of *Ax*NiR in the presence of phenol red has been used to allow the determination of both the rate of ET and the time-resolved measurement of proton uptake from the bulk solvent associated with a single turnover at pH 7 to be determined [68]. As observed in pulse radiolysis studies, the rapid reduction of the T1Cu (~3000 s^{-1}) was followed by a slower (244 s^{-1}) partial re-oxidation to establish redox equilibrium. In the presence of nitrite (10mM) essentially full oxidation of the T1Cu occurred but at a slower rate (104 s^{-1}). The corresponding rates of proton uptake were 305 s^{-1} in the absence and176 s^{-1} presence of nitrite indicating the close coupling of these processes. A rate-limiting protonation step has also been proposed for *Af*NiR where the rate of inter-Cu ET in turnover is significantly slower when compared with the rate in the absence of nitrite [35].

Two putative proton channel mutants of *Ax*NiR, one involving Asn90 and the other His 254 and the double mutant were active, but that of Asn90 was inhibited by 70%. Proton consumption in steady-state assays showed that two protons were consumed/nitrite reduced, indicating that even in the double mutant protons can access the active site [68]. In laser flash photolysis experiments inter-Cu ET to equilibrium was observed for the WT and the H254F variant and in the presence of nitrite the T1Cu was fully reoxidised. In contrast, both the N90S and the double mutant no ET occurred due to the 60 mV increase of the mid-point reduction potential of the T1Cu to +315 mV. In the presence of nitrite inter-Cu ET resulted in reoxidation of the T1Cu. The [nitrite] dependence of inter-Cu ET for the WT and the H254F variant show complex behaviour

with an initial drop at low concentrations before increasing at higher [nitrite], whereas the N90S and the double mutant show normal saturation kinetics. These data indicate that the Asn90 channel is the main source of protons to the active site and that when this channel is disrupted proton delivery becomes rate-limiting in turnover.

Their kinetic coupling was determined in a time-resolved pH-perturbation experiment in which turnover of $T1Cu^{+}$-$T2Cu^{++}$nitrite-bound *Ax*NiR species at pH 9 was initiated using stopped-flow to decrease the pH 7, a permissive value for ET [58]. The observed rate constants for ET were $377s^{-1}$ in H_2O and 502 s^{-1} in D_2O showing an inverted SKIE for inter-Cu ET of 0.75. This pattern is similar to that seen in laser-flash photolysis experiments where the inverted SKIE was attributed to the differential population of parallel reaction routes of the random sequential mechanism [57]. Given the close correlation of ET with proton uptake an important question arises as to the nature of the mechanistic trigger for PCET i.e. which comes first, ET or proton transfer?

The EPR features of the T2Cu-nitrite-$T1_{ox}$ species of *Rs*NiR exhibit a pH dependence interconversion of two species with a pK_a of 6.4 [42]. DFT modelling indicated the high pH form had deprotonated Asp_{CAT} and protonated $His_{CAT.}$ At ~pH 9 in the presence of nitrite EPR and absorbance measurements show the T1Cu centres of *Rs*NiR and *Ax*NiR can be selectively reduced by ascorbate/PMS [48, 61]. Resonance Raman spectroscopy showed the T1Cu was not perturbed by pH changes and the lack of ET was attributed to the reduction potential of the T2Cu being ~120 mV below that of the T1 site [42]. On lowering the pH to ~5, protonation of Asp_{CAT} to allows proton-coupled ET to initiate enzyme turnover resulting in complete oxidation of the T1Cu and the formation of free NO [42, 68] consistent with protonation occurring before ET in both blue and green prototypic CuNiRs.

6. Copper centres in damage-free crystal structures of prototypic CuNiRs

Despite the potential for high doses of synchrotron X-rays to cause radiation damage or initiate ET from hydrated electrons during data collection many SRX structures of CuNiRs show $T2Cu^{++}$ to have a $(His)_3H_2O$ ligand set in complete accord with ENDOR solution studies, indicating that irrespective of other changes, the first coordination sphere ligation of T2Cu is not changed by exposure to X-rays for the resting state of the enzyme. The primary effect is the reduction of the T1Cu site as assessed from on-line optical and XANES spectroscopic measurements on *Ax*NiR single crystal during crystallographic data collection [38, 51]. In the presence of nitrite, X-ray exposure necessary for high-resolution structure determination, turnover of the enzyme occurs prior to any noticeable radiation damage leading to mixture of states making the goal of providing a structure-based catalytic mechanism at the chemical level, a challenging task. The emerging methodology of X-ray free-electron laser (XFEL) crystallography allows data to be collected using femtosecond X-ray pulses, too short a timescale for any radiation-induced chemistry or ET to occur, allowing structures to be determined free from radiation-induced chemistry (FRIC).

Serial femtosecond crystallography (SFX) utilises data collection from thousands of micro crystals exposed to XFEL pulses of X-rays. This technique can be used in time-resolved studies but the small crystal size limits the resolution obtainable. The SFX approach has been applied to *Af*NiR and *Gt*NiR. A surprising feature of resting-state SFX structures of oxidized as-isolated *Af*NiR and *Gt*NiR was the absence of a water ligand of the T2Cu site and an unexpected variability in the ligand bound to the T2Cu

that is not evident in SRX structures. In the SFX structure of *Gt*NiR(1.43Å) a Cu ion (20%) bound to His_{CAT} and a sodium ion in the T2Cu pocket [69]. In the SFX structure of *Af*NiR (2.03Å) the T2Cu had a chloride ligand presumed to arise from purification/crystallization media, since the SRX structure showed H_2O as the apical ligand [70]. The effect of chloride in as a substitution for water as a T2Cu ligand is uncertain, but has been proposed to account for differences in the rotation and main chain H-bonding of the Nδ1 of His_{CAT} between SRX and SFX as-isolated structures of *Af*NiR (where differences are seen) [70] and Br^{2D}NiR (where they are not) [32]. In the case of Br^{2D}NiR His_{CAT} rotation and changes in H-bonding to Thr275 is only observed in the atomic resolution SRX-nitrite bound structure.

An alternative strategy to study damage-free enzyme and obtain FRIC structures is serial femtosecond rotational crystallography of a single crystal (SF-ROX) as was used for *Ax*NiR [71] *Ac*NiR [39] and Br^{2D}NiR (1.3Å) resolution [32]. A variety of T2Cu ligands have also been observed using this technique. *Ax*NiR was shown to have a dioxo-species proposed to be the one-electron reduced intermediate of the oxidase reaction leading to H_2O_2 as a product of dioxygen reduction by CuNiRs [71]. A di-oxo species generated by T2Cu reduction under aerobic conditions and assigned as a superoxide anion has been structurally characterised in *Gt*NiR [72]. A dual conformation of a single H_2O axial ligand of the T2Cu was observed in the anaerobic SRX structure compared with an earlier aerobic SRX structure showing a diatomic ligand [73]. In addition a peroxide-bound state of *Gt*NiR was generated by crystal soaking with H_2O_2 of the C134A T1Cu variant where inter-Cu ET is compromised. These FRIC structures complement earlier SRX data for *Gt*NiR (1.2Å) coupled with on-line spectroscopy at 100k showed progressive x-ray bleaching of T1Cu was accompanied by an increase in the 200-300 nm region, assigned to a LMCT transition of a dioxo species [73]. The T2Cu had a side-on diatomic molecule modelled as dioxygen/superoxide anion (O—O 1.25 Å; Cu—O 2.4, 2.13Å). These findings have clear relevance to the oxidase and superoxide dismutase activity shown by CuNiRs.

6.1 FRIC structures of ‘as-isolated’ prototypic CuNiR

The SF-ROX FRIC structures of *Ac*NiR [39] and *Br*^{2D}NiR [32] did have H_2O molecule(s) as T2Cu ligands thus providing a starting point for defining structural changes associated with the reduction or nitrite binding or NO binding following the chemical reduction of the substrate-bound enzyme crystals. The as-isolated, nitrite-bound and reduced SF-ROX structures *Ac*NiR at 100 K were complemented by a damage-free room temperature neutron structure of as-isolated enzyme [39]. The major difference between the global SF-ROX as-isolated oxidized, ascorbate-reduced and neutron structures was in the surface loop region associated with the binding of azurin and c-type CYT [74]. The loop is disordered in the as-isolated enzyme but becomes ordered in the reduced, and neutron structures. The SF-ROX structure of the as-isolated *Ac*NiR enzyme (1.5 Å) showed a single highly-ordered H_2O ligand at the T2Cu as seen in the SRX (0.9Å) structure [41]. In contrast to the SRX structure, two variants of the proximal conformation of Asp_{CAT} were evident resulting in modification of the H-bonding network to form a direct H-bond to the T2Cu H_2O ligand. Both proximal conformations were H-bonded by Oδ1 to the H_2O molecule linking His_{CAT}-Asp_{CAT}. The neutron structure (1.9 Å) showed T2Cu coordinated to a single D_2O molecule in a similar tetrahedral position as the H_2O ligand in the SF-ROX structure and Asp_{CAT} to be in a single proximal conformation. Nuclear density maps clearly showed that neither Asp_{CAT} or His_{CAT} of the resting enzyme are protonated at a pD of 5.4.

6.2 Damage-free FRIC structure of nitrite-bound prototypic CuNiR

The nitrite bound SF-ROX structure of the green *Ac*NiR at 1.5 Å resolution showed both 'top-hat' and 'side-on' nitrite conformations at equal occupancy associated with Asp_{CAT} adopting equal proximal and gatekeeper conformations [39]. The distorted proximal conformation seen in the as-isolated enzyme was not evident. Low-dose in-house data collection was used to probe the pH dependence over the range 5 to 6.5 on the mode of nitrite binding and associated changes to the T1Cu site. At pH 5 nitrite binding and Asp_{CAT} organization was comparable with the SF-ROX structure described above. Increasing the pH to 5.5 induces Met141 in the second coordination sphere of the T1Cu, to adopt two conformations at 50% occupancy to allow a partial H_2O to H-bond to T1Cu ligand His145 and create a water network to the protein surface. This process is complete at pH 6 and the original conformation of second coordination sphere Met141 is lost.

The FRIC structure of nitrite-bound *Br*^{2D}NiR was obtained using the SF-ROX approach and 28 large crystals to a resolution of 1.3 Å [32]. The binding of nitrite was confirmed by UV/vis micro-spectrophotometry on one of the crystals prior to XFEL irradiation. The most notable observation in this substrate bound XFEL-FRIC structure was the nitrite molecule at the $T2Cu^{2+}$ site in a single 'side-on' conformation with all 3 atoms O^1, N and O^2 binding by almost identical distances of 2.12 Å, 2.02 Å and 1.92 Å. The 'side-on' nitrite in this FRIC structure is in an ideal position to the full occupancy proximal Asp_{CAT}, with its O^2 atom 2.25 Å away from Asp_{CAT} Oδ2 atom. His_{CAT} has its imidazole ring and its $N^{\delta 1}$ atom rotated towards residue Glu274 carbonyl oxygen.

6.3 Structural movies of prototypic CuNiR in a single turnover

Starting with crystals with $T1Cu^{++}$-$T2Cu^{++}$ with nitrite bound CuNiR, multiple structures from the same volume of one crystal can be obtained using MSOX. Building on earlier SRX studies that showed X- ray photolysis resulted in ET to the T2Cu with nitrite bound [51], 'structural movies' of *Ac*NiR generated during progressive X-ray-induced single turnover of nitrite-soaked crystals at several temperatures including ambient temperature revealed mechanistically-relevant structures. They clearly showed sequential structures of T2Cu with nitrite, mixed nitrite and NO, side-on NO, and finally H_2O ligands [33, 75, 76]. The events revealed using this technique mirror solution studies of ET and proton uptake in the presence of nitrite described in section 5.

In MSOX series at 100K, the initial global structure of *Ac*NiR (1.07 Å resolution showed no significant difference from an earlier SRX structure at 0.9Å and remained unchanged throughout data collection indicating that enzyme turnover is not associated with significant changes in conformation while nitrite is bound [32]. In addition to providing the first experimental evidence for the operation of the sensor loop in catalysis, a single side-on Cu-NO and proximal Asp_{CAT} conformation were seen at the end of the series. These changes are the same as those first observed in the SRX structures (0.9 Å) of *Ac*NiR where dual conformations were observed for Asp_{CAT} when H_2O or nitrite were bound and only the proximal in the NO-bound T2Cu site [41]. The MSOX study also highlighted small changes in ten H_2O molecules forming a water chain spanning the T1 and T2Cu sites linking both to the bulk solvent, and proposed a five-residue proton

trigger loop connecting the His-Cys ET bridge to allow controlled delivery of protons to the T2Cu dependent on the redox state of the T1Cu. This study provided structural evidence for a stable side-on symmetrical binding conformation for NO produced in catalytic turnover, a binding mode consistent with a DFT study attributing it to steric interaction with Ile_{CAT} [77]. This is also consistent with EPR and ENDOR spectra of single turnover solution studies of *Rs*NiR identified a Cu+-NO species interacting with Ile_{CAT} [78].

An MSOX series at 170K of *Ac*NiR at atomic resolution allowed SHELXL unrestrained refinement to determine accurate structural detail of intermediates [31]. In frame 1, nitrite bound in a highly asymmetric bidentate mode with Cu—O of 1.88(3) Å and 2.51 Å respectively and Cu—N 2.42(6) Å at 0.75 % occupancy. Changes in the proximal and gatekeeper rotomers of Asp_{CAT} and the eventual formation of a side-on NO enzyme-bound product with Cu—O and Cu—N of 1.65(1) Å and 1.86(2) Å respectively. DFT modelling suggested both true $\{CuNO\}^{11}$ and formal $\{CuNO\}^{10}$ states may occur with the $\{CuNO\}^{10}$ state stabilised by the protonation state of His residues. The energy difference between side-on and end-on forms was compatible with side-on $\{CuNO\}^{11}$ being formed in the active site pocket but not necessarily in synthetic complexes except at low temperatures [31].

7. Chemically-induced enzyme turnover of damage-free prototypic CuNiR

A recent development has been the determination of XFEL-FRIC structures of nitrite- and NO-bound enzyme and also new intermediate species generated in a single turnover for the blue Br^{2D}NiR using dithionite as a reductant [32]. A stopped-flow study of the reaction of *Ax*NiR with dithionite showed that the reductant was the radical $SO_2^{\cdot-}$ formed by the dissociation of the parent ion $S_2O_4^{2-}$ and kinetic analysis showed the T1Cu was reduced directly [50]. Crystals of Br^{2D}NiR with full nitrite occupancy was subject to a time-dependent soak with dithionite to initiate catalysis. The oxidation state of the T1Cu was monitored throughout using on-line spectroscopy. The structures obtained provide additional insight to catalytic events captured by MSOX molecular movies of *Ac*NiR. The use of dithionite effectively generates an anaerobic environment in the crystal removing any suggested ambiguity, (arising from adventitious binding dioxygen) [72], in the assignment of T2Cu electron densities to ligand speciation in SFX and MSOX studies. A clear LMCT absorption band from at from nitrite bound to the T2Cu is also observed at ~360 nm in the optical spectrum of the single crystal.

The comprehensive structural study of the blue Br^{2D}NiR in which very high resolution SRX (1.1Å) was combined with SHELXL unrestrained refinement and XFEL structures of key intermediates of the catalytic cycle enabled the formulation of a detailed structure based scheme for nitrite reduction in prototypic CuNiR turnover [31]. SHELXL refinement made possible by the very high atomic resolution of the structures, enabled determination of bond lengths and angles to a high level of precision allowing protonation states of active site residues to be assigned. The SRX structure showed two distinct conformers of the active site. One with two H_2O molecules (W1 and W2 both at 0.67 occupancy) bound to the T2Cu and Asp_{CAT} in the proximal conformation, and a second with a single H_2O (W3 at 0.33 occupancy) and Asp_{CAT} in a distorted proximal conformation first seen in XFEL structures of *Ac*NiR [41]. Estimates of the carboxyl bond lengths of Asp_{CAT} in these conformations were consistent with the distorted proximal

conformation being protonated. In both conformations the H-bonds to His_{CAT} and the T2Cu ligands W1 or W3 are retained. The C-N-C bond angles of His_{CAT} are consistent with protonated Nδ1 (H-bonded to the carbonyl of main chain Glu^{274}) and non-protonated Nε2.

The XFEL-FRIC structure of Br^{2D}NiR (1.3Å) of nitrite-bound enzyme showed a single, previously unobserved side-on conformation of nitrite with all three atoms at very similar distances to the T2Cu of 2.12, 2.02 and 1.92 Å. The positions of the O atoms are close to those of the 'top-hat' conformation seen in the SRX structure.

Following incubation of a nitrite-bound crystal with dithionite a side-on bound NO was observed in the SRX structure (1.19Å) allowed SHELX refinement. The side-on coordination mode was slightly asymmetric 2.17(4) Å and 2.08(3) Å for Cu—N and Cu—O respectively. Asp_{CAT} was in the proximal conformation with bond lengths consistent with protonation at Oδ2 and Oδ1 H-bonded to the bridging H_2O to His_{CAT} Nε2. The imidazole of His_{CAT} was H-bonded to Glu274 carbonyl from Nδ1 as in the as-isolated enzyme.

The XFEL-FRIC structure of NO-bound Br^{2D}NiR generated by incubation of nitrite-bound crystal with dithionite (100K) was obtained by using 55 large crystals with SF-ROX method of serial crystallography. We were able to obtain a resolution of 1.3Å for this structure, which captured three T2Cu species arising from chemically-induced turnover, NO-bound, ligand-free and H_2O-bound. The side-on coordination mode of NO (occupancy 0.4) was more asymmetric than seen in the SRX structure with 2.47 Å and 2.12 Å for Cu—N and Cu—O respectively. Asp_{CAT} was in the proximal conformation. In the H_2O- bound site (occupancy 0.3), the Cu—O was 2.07 Å and H-bonded to Asp_{CAT} 2.16 Å. In the ligand-free structure Ile_{CAT} was flipped towards the Cu in a previously unseen conformation (occupancy 0.3) which because of steric constraints is only possible when H_2O or NO are not in the active site pocket.

7.1 Structure-based mechanism

In the context of the mechanism of CuNiRs the distinction between OH^- and H_2O bound to the T2Cu of the resting enzyme are important. The former is a proposed end product in a mechanism that does not involve a Cu-nitrosyl intermediate, and the latter a solvent-derived ligand that binds following NO release from the T2Cu active site. Computational studies have not resolved which of these alternatives is involved in enzyme turnover but there is general agreement that nitrite binds to the T2Cu by displacement of the H_2O/OH^- ligand. It has been shown that the T2Cu in the SRX structure of *Ac*NiR (0.9 Å) [41], the SF-ROX (1.5 Å) and the neutron structure of per-deuterated enzyme (1.8 Å) [39] all have a single neutral $H(D)_2O$ ligand rather than the D_3O or OD^- ion which have been proposed as possible alternatives. This assignment is supported by proton uptake measurements during steady-state turnover of *Ax*NiR in the presence of pH indicator phenol red, which unambiguously showed that two protons are coupled to nitrite reduction [51] indicating that the catalytic Cu has H_2O bound rather than OH^- in both blue and green CuNiRs. The MSOX studies at a variety of temperatures including room temperature show unequivocally that when the reaction *in crystallo* is initiated from a $T2Cu^{++}NO_2^-$ complex a Cu-nitrosyl is formed and NO is released as the enzyme resumes the resting state in the 'binding before reduction' route of the random sequential mechanism, which we propose should be called alternate sequential mechanism or simply ordered mechanism where two alternate routes are available. In

both cases, enzyme undergoes reaction in an ordered manner and follows a particular route, see figure 8.

INSERT Figure 8 here

The significance of the experimentally observed NO species in CuNiR during turnover in crystals has been questioned as possibly arising from a product-inhibited form or an intermediate in the reductive coupling reaction to form N_2O observed in the presence of excess NO [9]. The formation of a Cu-nitrosyl species during catalysis has been demonstrated in EPR/ENDOR studies of *Rs*NiR [78]. On incubation of the as-isolated enzyme with a 2-fold molar excess of nitrite and NADH/PMS (pH 7.2) an EPR spectrum with considerable hyperfine lines near g = 2.00 (g_x=2.044, g_y=1.998 and g_z=1.923) developed. The fast spin relaxation of this species required temperature below liquid nitrogen to enable its detection, similar to {CuNO}^{11} models. It was assigned to a T2Cu$^+$-NO$^\cdot$ adduct very similar to that formed by exposure of RsNiR to low concentrations of endogenous NO [48]. Spin integration of the signal was 30-45% of the initial intensity and the question arises is this an intermediate in catalysis or an initial enzyme-substrate complex of the reverse reaction?

Most mechanistic studies of CuNiR have focussed on the forward reaction, the reduction of nitrite to NO, rather than the reverse reaction, which becomes significant at high pH values [79]. Reversibility was established by the effects of [nitrite] on an *Af*NiR-catalysed redox equilibrium of pseudoazurin/ NO [100 μM], a large excess of NO over [enzyme], but the enzyme bias is dependent on the redox potential of the donor/acceptor. When pseudoazurin (Em~ +275 mV) is replaced by NAD/NADH (E_m -320 mV) [48], the ratio becomes a very fine balance. At an enzyme:NO of 1:2 a nitrite-bound T2Cu species was formed due to the reverse reaction. However at a 10:1 excess of *Rs*NiR : NO the time course of the reaction monitored by EPR over 18 s showed initial formation of a T1Cu$^+$T2Cu$^+$-NO$^\cdot$ adduct which in the presence excess NO catalysed N—N bond formation to form free N_2O and *Rs*NiR in the mixed oxidation state T1Cu$^+$ T2Cu^{2+}. These findings are relevant to steady-state studies in which CuNiR is catalysing the reduction of nitrite, since the nitrosyl intermediate reacts with free NO to produce N_2O. Isotopic labelling established that a ^{15}N atom of nitrite is incorporated into N_2O [18, 80] placing the T2Cu$^+$-NO$^\cdot$ adduct as a catalytic intermediate, in line with the crystallographic MSOX data which show the formation and subsequent release of NO to yield the resting H_2O liganded state of the T2Cu.

Mutagenesis of two highly conserved residues Asp_{CAT} and His_{CAT} in the active site pocket of several CuNiRs, profoundly decrease catalytic activity and the binding affinity of nitrite. These residues have pK_a values that straddle the pH optimum for activity and have been assigned essential role in the delivery of protons to nitrite bound to the T2Cu. In addition, the role of Asp_{CAT} in substrate guidance and anchoring is clear in the structural movies of catalysis by *Ax*NiR, *Ac*NiR and *Br*NiR. For the vast majority of CuNiRs, both prototypic and extended variants, this is a reasonable scenario for functionality but the recent characterisation of the 3D-*Ts*NiR [44], in which a Ser residue replaces Asp_{CAT} indicates that it is not universal and raises the possibility that Asp_{CAT} is not directly involved in proton transfer. In this context the Asp98Ala variant of *Ax*NiR is particularly interesting. This substitution decreases the steady-state activity by 98% [81]

and no ET is detectable in pulse radiolysis experiments. However, in the presence of nitrite partial recovery of $T1_{ox}$ occurs with a k_{ET} of $3000s^{-1}$ some 10-fold higher than the WT enzyme [82] suggesting that ET is decoupled from proton uptake from the bulk solvent. The rapid partial oxidation of the T1Cu is suggestive of single-site reactivity in this mutant.

8. Domain extended CuNiRs

These enzymes are widely distributed in nature and have a prototypic CuNiR core with tethered cupredoxin or heme domains [see 11, 83, 84, for reviews]. The overall organisation of these to the catalytic core in different enzymes is shown in Figure 2. The initial expectation was that these extended CuNiRs arose as a consequence of evolutionary pressure driving gene fusion to link the genes of the azurin/pseudoazurin or cyt*c* electron donors to NirK leading to an enhancement of inter-protein ET. We still have much to learn about these types of CuNiR but studies to date have revealed a more complex interaction as discussed below.

8.1 Cupredoxin-extended CuNiR

Both N- and C- extended variants of CuNiR have been characterised.

8.1.1.N-terminal tethered

For many years the enzyme from *Hyphomicrobium denitrificans* A3151 (Hd_{A3151}NiR) was the single example of a core CuNiR with an additional N-terminal tethered cupredoxin domain containing a green T1Cu potential electron-donating centre to the blue T1Cu of the core enzyme. The crystal structure of this 3D-CuNiR (2.2Å) showed a hexameric structure formed by non-covalent head-to-head interaction of two trimers [85]. Recently, a CuNiR with 84% sequence identity was isolated from a second strain *H. denitrificans* 1NES1 (Hd_{1NES1}NiR) and characterised) showing a vey similar structure (2.05Å [86]. (FIG 9) The head-to-head arrangement of two trimers to form a hexamer in these enzymes differs from the prototypic hexameric structure of the anammox bacterium KSU-1. In the latter enzyme, the hexamer of covalently linked Cys—Cys trimers has a tail-to-tail interaction, and disruption into trimers by mutation resulted in an 80% loss of activity [13]. This contrasts with Hd_{A3151}NiR where trimer formation induced by mutation of the T1Cu site in the additional domain does not significantly effect $k_{CAT.}$

The structure of Hd_{1NES1}NiR provided clear evidence for a role of His 27 in the N-terminal peptide changing conformation on the displacement of the T2Cu H_2O ligand to provide water-mediated anchoring of nitrite at the catalytic T2Cu site, in addition to that provided by interaction with Asp_{CAT} [86] (see section 7). There were differences in the water occupancy of the proton channel from the T2Cu to solvent inter-monomer interface compared with Hd_{A3151}NiR [85].

INSERT Figure 9 here

8.1.2. Inter-Cu ET

The reduction of the T1Cu centres of Hd_{A3151}NiR by pulse radiolysis in the absence of nitrite is biphasic [87]. Kinetic difference spectra 200 μs after reduction were consistent with the fast phase being reduction of the greenT1Cu centre of the additional domain, as expected from its greater exposure to bulk solvent. The reduction rates of variants with selective inactivation of the two T1Cu sites by Cys to Ala substitution supported this

assignment. The organisation of the blue T1Cu and T2Cu centres in the core of *Hd*NiRs are very similar to prototypic CuNiRs with a single H_2O, H-bonded to Asp_{CAT} His_{CAT} linker. In the hexameric structure the solvent-exposed T1Cu of the extra domain is 24 Å from the nearest T1Cu centre in the catalytic core of an adjacent monomer too far for effective rates of ET. In addition, with reduction potentials of +353 mV and +345 mV for the green and blue T1Cu centres of there is little driving force for ET from the tethered cupredoxin domain to the core enzyme. This is consistent with a pulse radiolysis study of Hd_{A3151}NiR that showed no detectable inter-Cu ET over the pH range 4.5 to 7.5 [88]. This changed in the presence of nitrite and at pH 6 the k_{ET} was 2.4 x 10^{-2} s^{-1} some 10-fold slower than *Ac*NiR and *Ax*NiR. Over the same pH range the ET rate of the Cys/Ala T1Cu site variant of the tethered domain is 10^4-10^5 faster than the WT enzyme. The slow rate in the WT enzyme was attributed to the preferential reduction of the T1Cu of the cupredoxin domain some 24 Å from the T2Cu centre of the adjacent monomer. In contrast to the bell-shaped curve of prototypic CuNiRs. the pH-dependence of ET was markedly different, decreasing monotonically over the range pH 4.5 to 7.5, highly suggestive of a different mode of proton delivery in WT Hd_{A3151}NiR. This pH dependence of the rate of ET was also reflected in activity with *k*cat showing the same dependence [88].

Stopped-flow studies of the CYT*c*555 electron donation to Hd_{A3151}NiR showed biphasic kinetics and mutagenesis studies showed the fast 1.4 x 10^5 M^{-1} s^{-1} reaction was donation to the T1Cu of the core enzyme (80% of the amplitude), and the slower 9.4 x 10^3 M^{-1} s^{-1} to the T1Cu of the tethered domain [89].

In summary, in the presence of nitrite, the 10^4-fold faster rate of ET shown by the trimeric C114A variant suggests that in WT enzyme the electron primarily reduces the T1 site in the additional domain compromising ET to the T1Cu of the core enzyme. The effectiveness of CYTc551 in supporting activity of the WT Hd_{A3151}NiR suggests direct ET to the core. The novel bidentate η^2-N, O binding mode for a native CuNiR (see section 8.1.3) may be reflected in the unusual pH dependence of inter-Cu ET and activity and the lack of inter-Cu ET in the absence of nitrite suggests that a 'binding-before-reduction' branch of the alternate sequential mechanism operates. In the case of Hd_{1NES1}NiR when the reaction is initiated by the addition of enzyme to the assay there is a 200 s lag before the rate of NO formation becomes linear [86]. Pre-incubation with nitrite resulted in a linear rate and a ~ 5-fold increase in the steady-state rate of NO formation. Clearly slow event(s) occur in the resting enzyme, priming the enzyme before it reaches the catalytic active state.

8.1.3. Nitrite and NO bound structures

The SR structure of nitrite-soaked crystals of Hd_{1NES1}NiR (2.1Å) showed displacement of the T2Cu H_2O ligand, replaced in two of the three T2Cu sites of a trimer by nitrite and in the third by NO [86]. The nitrite binding mode differs from prototype CuNiR in being bidentate η^2-N,O binding with Cu-N and Cu-O distances of 1.9 and 2.0 Å respectively. The H_2O network in the active site pocket changes when nitrite is bound. His27 of the N-terminal peptide rotates to face the T2Cu to form H-bonds with two H_2O molecules W2 and W3 that also form H-bond with the bound nitrite (W2) and to Asp_{CAT} (W3), figure 9. In the NO- bound state His27 rotates away from the T2Cu and is no longer H-bonded to

a H_2O network. The NO binding is side-on, very similar to *Ac*NiR with Cu-N and Cu-O distances of 2.0 and 2.5 Å.

8.2. C-terminal tethered CuNiRs

A third member of cupredoxin-extended 3D-NiR family, a C-terminal tethered CuNiR has been isolated from the thermophilic bacterium *Thermus scotoductus* SA-01 (*Tc*NiR) and the structure (1.63Å) determined [44] (figure 2). In contrast to the of N-terminal cupredoxin-extended *Hyphomicrobium* enzymes, *Ts*NiR is trimeric. The orientation of the additional domain to the core enzyme is not seen in other extended CuNiRs since it interacts directly within the same subunit. As a consequence the twoT1Cu sites are separated by 14.1 Å and a clear putative ET route involving the T1Cu ligand His431 bridged by a H_2O molecule to Glu385 to the T1Cu ligand His125 of the core. The T1Cu ligand set is stellacyanin-like (His_2-Cys-Gln) in the additional domain, and has not been seen previously in CuNiRs. The T2Cu connects *via* a Cys-His bridge to the T1Cu and has a single H_2O as the apical ligand. In the active site pocket Val_{CAT} replaces the more usual Ile_{CAT}. A remarkable feature of *Tc*NiR is the absence of Asp_{CAT} in the sensor loop connection to the T1Cu seen in all other CuNiRs and plays a central role in our understanding of CuNiR functionality. A replacement Ser_{CAT} forms a H-bond to the T2Cu water ligand and via a $(H_2O)_4$ chain to His_{CAT}. It is also part of a putative proton channel from the T2Cu active site pocket to bulk solvent, Ser_{CAT} $(H_2O)_4$ Ala116$(H_2O)_2$Gly91Asn92. The H_2O molecule that bridges Asp_{CAT} and His_{CAT} in prototypic CuNiRs is missing. With a steady-state rate for nitrite reduction of 65 s^{-1} and an apparent K_M value for nitrite of 27μM this enzyme presents a challenge to the established view of the central role of Asp_{CAT} in functionality of CuNiR since, for example, the corresponding values for *Ax*NiR are 89 s^{-1} and 27μM.

9. C-terminal Heme-extended CuNiR

Recent genome comparisons have identified variant *nirK* with additional C-terminal monoheme domain in α, β and γ-proteobacteria indicating a widespread distribution [15, 82]. Two enzymes of this class, those from *Ralstonia pickettii* (*Rp*NiR) and *Pseudoalteromonas haloplanktis* TAC125 (*Ph*NiR) have been isolated and have been biochemically and structurally characterized (*Rp*NiR (1.01 Å), *Ph*NiR(1.95 Å) [89, 90, 91, reviewed in 84]. The two enzymes are trimers with similar core structures with a tethered N-terminal cytochrome domain. Although there are differences in the long 36 residue tethering link and its interaction with the core and the additional domain, in both cases the T1Cu is ~10 Å from the heme of the adjacent subunit. Two potential proton pathways to the T2Cu have been identified, one of which is formed between two adjacent monomers is also the substrate access channel. In contrast to prototypic CuNiRs this channel lacks H_2O molecules and is blocked by Tyr323 in *Rp*NiR (Tyr313 in *Ph*NiR) of the tethering link. This residue is conserved in all known heme-CuNiR sequences. The T2Cu site at the bottom of the channel has a single apical H_2O ligand H-bonded to Asp_{CAT} but in *Rp*NiR is also H-bonded to a second H_2O molecule a feature not seen in prototypic CuNiRs or in *Ph*NiR. An unusual feature of *Rp*NiR is the inability of the $T2Cu^{++}$ to bind nitrite as assessed from the lack of significant changes to the EPR spectrum and inability to diffuse nitrite into crystals [89]. Surprisingly pre-treatment of crystals with NO resulted in an opening of the channel due to the rotation of Tyr323

away from Asp_{CAT} and allowed the structure of the NO-bound enzyme to be determined. Similar NO-treatment of the Asp_{CAT} D97N variant allowed nitrite to bind and the structure determined [90]. The positioning of Tyr323 is not controlled by the T2Cu redox chemistry or that of the heme.

A reverse engineering approach of deconstructing *Rp*NiR into its catalytic core and cytochrome domain has proved a powerful tool in revealing the extent to which the additional domain modulates activity [92]. The structure of the core (2.25 Å) compared with WT is more compact and the previously blocked substrate access channel is open. This allows nitrite to be diffused into crystals without mutation/pre-treatment with NO and enabled the nitrite-bound and NO structures to be determined. The tethering link changes from random coil seen in the intact enzyme to β-strand adjacent to surface of adjacent monomer and stabilised by salt bridge of Tyr323 and Glu44 an arrangement similar to prototypic CuNiRs. Utilising this position of the tethering link an extended model for the solution structure of WT *Rp*NiR was developed that produced an excellent fit to small-angle x-ray scattering (SAX) data [92], in contrast to the poor fit based on the compact WT *Rp*NiR structure [89] Fig 10.

INSERT Figure 10 here

The heme domain is solvent exposed with the extended tethering link to the core enzyme resulting in an average heme-T1Cu distance of ~40 Å providing an explanation for the slow rate of ET from reduced heme to T1Cu. This points to the role of conformational dynamics that enables the tethered domain with the linker to move from the extended structure (observed in SAXS) and compact structure where the Tyr323 locks in the catalytic pocket as observed in the crystallographic structures. Further experimental and computational work on this and other tethered CuNiRs is required to map out the conformational dynamics pathway and its role in determining catalysis. Whether such conformational dynamics is common to other tethered CuNiRs including *Hd*NiR remains to be investigated.

9.1 Heme and Inter-Cu electron transfer

Pulse radiolysis studies of *Ph*NiR in the absence of a mediator showed reduction of heme and the subsequent establishment of a redox equilibrium with the T1Cu with a rate of 5.5 x 10^3 s^{-1}, considerably slower than the expected rate (10^9 s^{-1}) for two centres 10 Å apart [88], but consistent with the extended SAXS model of *Rp*NiR. The equilibrium position of ~ 50% is consistent with the reduction potentials being close together, as is the case for *Rp*NiR (heme, +290 mV, T1Cu +266mV) [92]. In the presence of mediator the T1Cu of *Ph*NiR was rapidly reduced but ET to the T2Cu did not occur unless nitrite was present, but even then only 30% recovery of oxidised T1Cu was observed, suggestive of one-third-site reactivity. A similar finding that the rate-limiting rate constant for the oxidation of reduced *Rp*NiR by nitrite was three times lower than that of the steady-state was consistent with 'one-third site reactivity' in turnover [92]. Computational study of *Rp*NiR showed the positions of Cu and Asp_{CAT} were fixed in the timeframe of MD (7 ns) calculations of conformational variation showed flexibility of the channel allowed movement of Tyr323 to open the channel in one of the three subunits [93].

Laser flash photolysis studies of *Rp*NiR also showed an incomplete and slow rate of ET from heme to T1Cu of 16.8 s^{-1} [92]. Only 5% of the expected 38% of the T1Cu was

reduced indicting that thermodynamic equilibrium was not established, attributed to rate-limiting searches of conformational space to optimize electronic coupling between the two centres. The reduction of the heme in the presence of nitrite promotes inter-Cu ET, attributed to the increase in T2Cu reduction potential on nitrite binding. Although pre-incubation of *Rp*NiR with dithionite reduced the heme and the enzyme was not inactivated, presumably Tyr323 in the substrate access channel blocked access to SO_2.- an analogue of nitrite and inter-Cu ET does not occur in the absence of nitrite. The *Rp*NiR core also showed no ET unless nitrite was present, consistent with the mid-point reduction potentials of +331 and +243 mV for the T1 and T2Cu centres respectively. The [nitrite] dependence shows the same complex pattern seen for *Ax*NiR, see section 5.3. in contrast to WT *Rp*NiR that shows Michaelis-Menten behavior. The lack of inter-Cu ET in the absence of nitrite suggests that a 'binding-before-reduction' branch of the alternate sequential mechanism operates in *Rp*NiR, as is the case in *Hd*NiR [see section 8.1.2.].

9.2 Nitrite and NO bound structures

The nitrite-bound structure of the *Rp*NiR D97N variant showed binding in a bidentate η^2-N,O mode with Cu-N and Cu-O distances of 1.8 and 1.9 Å respectively with the non-coordinated O atom at 3Å [90]. The N co-ordinated mode seen here and in *Hd*NiR is the preferential mode indicated by computational chemistry (see [9]). A more recent quantum mechanical/molecular mechanical study suggested that Tyr323 acts as a flexible gatekeeper that in the resting enzyme can be displaced by H_2O dynamics to open the substrate access channel [93]. The relative stabilities of N-bound and 'top hat' binding modes of nitrite to $T2Cu^{++}$ were ambivalent but for the reduced site there was a clear preference for N-binding [56].

The NO-bound structures of *Rp*NiR and the D97N variant showed the side-on conformation with Cu-N and Cu-O distances of 2.0 Å and 2.6 Å for WT and 2 and 2.8 respectively, with a probable H-bond to Asp_{CAT} 3.1Å. The binding of NO results in a 90^o flip of the side chain of Ty323 disrupting the H-bond to Asp_{CAT} to form a new H-bond with Gly109. This results in movement of the tethering link of the core enzyme to the heme domain opens the blocked channel from the T2Cu to bulk solvent. The position of the link in as-isolated *Ph*NiR is intermediate with Tyr313 free to flip without any steric constraints suggesting they represent two conformations of the tethered complex. Three substitutions of Typ323 (Y323A/F/E) were constructed to test its importance in controlling access to the active site [92]. All had ~90% activity of the WT enzyme and crystals were amenable to nitrite soaking. The nitrite-bound structures showed displacement of the H_2O ligand and showed bidentate η^2-O, O mode to the T2Cu with 'side-on' and Y323A a previously unobserved 'inverse hat' mode. These binding modes differ from the η^2-N, O mode in the D97N variant described above.

10. N-terminal tethered 4-domain CuNiR with cupredoxin and heme-extensions

This enzyme has been identified in several members of the order *Rhizobiales,* which in addition to this extended CuNiR also have a *nirK* gene encoding a prototypic CuNiR.[16] Both the 4-domain (Br^{4D}NiR) and the 2D-CuNiR (Br^{2D}NiR) and enzymes from *Bradyrhizobium* sp. ORS 375 (*Br*NiR) have been characterized, and the SR and XFEL-FRIC structures of Br^{2D}NiR have been determined to atomic resolutions [32], see section 6. To gain insight to the role of the tethered domains in Br^{4D}NiR a reverse engineering approach has been used to generate domain deletions that correspond to the N-terminal

cupredoxin-extended *Hd*NiR and the double Δ(Cyt*c*-Cup) *Br*^{4D}NiR enzyme [16]. corresponding to a prototypic 2D-CuNiR enzyme. Size exclusion chromatography showed the WT to be a hexamer/ trimer mixture with the hexamer predominating. On removal of the heme domain the trimer became the predominant species. The double domain deletion Δ(Cyt*c*-Cup) *Br*^{4D}NiR showed a monomer/dimer mixture with the monomer predominating. This behavior shows a clear role of the additional domains in stabilizing the hexameric form of the WT enzyme, similar to that in *Hd*$_{A3151}$NiR where the cupredoxin domain stabilises the hexamer [85]. The amino acid sequence alignment showed conservation of residues ligated to the T1 and T2Cu, Asp$_{CAT}$, His$_{CAT}$ and Ile$_{CAT}$. Construction of the D439N variant resulted in a 97% loss of activity indicating its importance for catalysis. The activity of *Br*^{4D}NiR is 25% that of Br^{2D}NiR which is ~20-fold lower than typical prototypic CuNiRs. It is not clear to what extent the equilibria discussed above are reflected in activity assays. The Δ(Cyt*c*)*Br*^{4D}NiR enzyme where the trimer is dominant shows a lag of ~900 s before linear rates of NO formation are observed. Pre-incubation of the enzyme with ascorbate for 600 s eliminates the lag and increases the activity.

The structure of the Δ(Cyt*c*-Cup) core enzyme was most similar to the core of *Hd*NiR. The T2Cu had a single H_2O apical ligand and the T1CuCys-HisT2Cu ET pathway was conserved. A significant difference was in the H_2O structure around the active site pocket with many H_2O molecules missing.

The domain arrangement of the variants discussed above is shown in Fig 2. This altered landscape of the architecture of CuNiRs poses interesting questions as to whether all the redox centres in the additional domains are competent in ET to the core enzyme. In this role, the expectation would be that allowing the enzyme to function without the necessity of exploring 'encounter-complex' space for transient complex formation with a cupredoxin/cytochrome physiological electron donor would enhance activity. To date, structural studies of *Rp*NiR and *Tc*NiR show separation of the heme-T1Cu site of the core enzyme of ~10 Å to facilitate effective ET. This is not the case with the *Hd*NiRs where the separation is ~20 Å, too far to allow reasonable rates of ET and thus significant conformational rearrangement would be required if this tethering is relevant for catalysis. Mutational, biophysical and reverse engineering studies also indicate complex roles of tethering requiring a multi-disciplinary approach. In the C-terminal heme tethered system the in-out requirement of Tyr323 from the catalytic pocket and potential large-scale conformational dynamics with unravelling of the linker that carries Tyr323 need further investigation.

11. Outlook

The apparent simplicity of the reversible reduction/oxidation reactions, coupling the transfer of one electron to the uptake of two protons catalysed by CuNiRs has provided research opportunities for the application and development of emerging techniques. The widespread distribution of cupredoxin- and heme-extended variants opens up new opportunities for studying regulation of activity and interdomain electron transfer. The identification of an active CuNiR with the Asp$_{CAT}$ substitute with Ser$_{CAT}$ effectively rules out a mechanism involving a deprotonated Ser$_{CAT.}$ In this enzyme only one putative proton channel has been identified connecting Ser$_{CAT}$ to bulk solvent. In this context is useful to note that the low activity phenotype of Asp$_{CAT}$D98N variant of *Ax*NiR is essentially corrected when azurin is used as an electron donor. The availability of X-ray free electron lasers (XFEL) have provided a paradigm shift in the form of a variety of

serial crystallography approaches which is allowing damage-free FRIC structures to be collected as well as room temperature by injecting thousands of crystals in the XFEL beams for single shot experiments. Some of these serial crystallography approaches are now emerging on advanced synchrotron facilities [94] that would help utilisation of these for wider number of systems at a variety of temperatures including room temperature. This, together with single crystal spectroscopy, would help better integration of spectroscopic and structural data. This parallel is expected to expand to rapid mixing SFX experiments [95] so that real time reactions can be structurally defined, and for example, may enable the 'reduction-before-binding' route of the random sequential mechanism to be accessed.

Acknowledgements.

We would like to thank BBSRC (e.g. BB/N013972/1, BB/L006960/1, BB/G005869/1, BB/D016290/1, 719/B06916) and STFC for their support over three decades of our research on nitrite reductases. We also acknowledge RIKEN for their support for several PhD students during their extended stay at Harima campus through Liverpool-RIKEN partnership. We thank Dr. Masaki Yamamoto and Prof. Yoshitsugu for hosting our joint students. We are grateful to current and past members of the Molecular Biophysics Group including several PhD students and postdoctoral fellows particularly Samuel Rose, Daisuke Sasaki, Thomas Halsted, Sam Horrell, Mark Ellis and Fraser Dodd. We are also indebted to our colleagues, Dr Svetlana Antonyuk, Dr Richard Strange and Dr. Michael Hough for several years of in-depth discussions and several significant publications.

In the context of this special issue RRE wishes to recognise the collaboration with Prof Isabel Moura in the co-supervision of Miguel Prudencio in his PhD studies on nitrite and nitrous oxide reductases some 20 years ago.

References

[1[W. G. Zumft, Cell biology and molecular basis of denitrifcation, Microbiol. Mol. Biol. Rev., 61 (1997) 533–616.

[2] K. M. Lancaster, J. D. Caranto, S. H. Majer , M. A. Smith, Alternative Bioenergy: Updates to and Challenges in Nitrification Metalloenzymeology, Joule 2, (2018) 421–441.

[3] D. Hera, H. Toh, C.T. Migita, H. Okubo, T. Nishiyama, M. Hattori, K. Furukawa, T. Fujii, Anammox organism KSU-1 expresses a NirK-type copper-containing nitrite reductase instead of a NirS-type with cytochrome cd1, FEBS Lett., 586 (2012) 1658-1663.

[4] A. R. Ravishankara, J. .S Daniel, R. W. Portmann, Nitrous oxide (N_2O): the dominant ozone-depleting substance emitted in the 21st century. Science (2009) 326 123–125.

[5] M. Whiley, N. Goire, M. M. Lahra, B. Donovan, A. E. Limnios, M. D. Nissen, T. P. Sloots, The ticking timebomb:escalating antibiotic resistance in *Neisseria gonorrhoeae,* J. Antimicrob. Chemo. 67 (2012) 2059-2061.

[6] M. Yamamoto, M. Nagao, G. Hotta, Y. Matsumura, A. Matsushima, Y. Ito, S. Takaakura, S. Ichiyama, Molecular characterisation of IMP-type metallo-β-lactamases among multidrug-resistant *Acromobacter xylosoxidans* J. Antimicrob. Chemo. 67 (2012) 2110-2113.

[7] M.A. M Jamali, C. C. Gopalasingam, R. M. Johnson, T Tosha, K. Muramoto,S. P. Muench, S. V. Antonyuk, Y, Shiro, S. S. Hasnain, The active form of quinol-dependent nitric oxide reductase from *Neisseria meningitidis* is a dimer, IUCrJ 7 (2020) 404-415.

[8] J. K. Bower, A. Y. Sokolov, S Zhang, Four-coordinate copper halonitrosyl $\{CuNO\}^{10}$ complexes, Angew. Chem., Int. Ed., 58 (2019) 10225–10229.

[9] E. I. Solomon, D. E. Heppner, E. M. Johnston, J.W. Ginsbach, J. Cirera, M. Qayyum, M. T. Kieber-Emmons, C. H. Kjaergaard, R. G. Hadt, L. Tian, Copper active sites in biology, Chem. Rev., 114 (2014) 3659-3853.

[10] M. Nojiri, Structure and function of copper nitrite reductase, In: I. Moura, J.J.G. Moura, S.F. Pauleta, L.B. Maia (Eds.) Metalloenzymes in Denitrification : Applications and environmental impacts, The Royal Society of Chemistry (2017) pp.91-113.

[11] S. Horrell, D. Kekilli, R. W. Strange, M. A. Hough, Recent insights into the function of copper nitrite reductases, Metallomics 9 (2017) 1470-1482.

[12] T. J. Lawton, K. E. Bowen, L. A. Sayavedra-Soto, D. J. Arp, A. C. Rosenzweig, Characterisation of a nitrite reductase involved in nitrifyer denitrification, J. Biol. Chem. 288 (2013) 25575-25583.

[13] D. Hira, M. Matsumura, R. Kitamura, K. Furukawa, T. Fujii, Unique hexameric structure of copper-containing nitrite reductase from an anammox bacterium KSU-1, Biochem. Biophys. Res. Comm. 526 (2020) 654-660.

[14] H. Ichiki, Y. Tanaka, K. Mochizuki, K. Yoshimatsu, T. Sakurai, T. Fujiwara, Purification, characterization and genetic analysis of a Cu-containing dissimilatory nitrite reductase from a denitrifying halophilic Archaeon *Haloacula marismortui,* J. Bacteriol. 183 (2001) 4149-4156.

[15] H. Decleyre, K. Heylen, B. Tytgat, A. Willems Highly diverse *nirK* genes comprise two major clades that harbour ammonium-producing denitrifiers, BMC Genomics 17 (2016) 1-113.

[16] D. Sasaki, T. F. Watanabe, R. R. Eady, R. C. Garratt, S. V. Antonyuk, S. S. Hasnain, Reverse engineering of a novel 4-domain copper nitrite reductase reveals functional regulation by protein-protein interaction, FEBS J. 288 (2021) 262-280.

[17] T. Kakutani, Watanabe, K. Arima, T. Beppu, A blue protein as an inactivating factor for nitrite reductase from *Alcaligenese faecalis* strain S-6, J. Biochem. 89 (1981) 463-472

[18] C. L. Hulse, B. A. Averill, J. M. Tisdje Evidence for a copper nitrosyl intermediate in denitrification by copper-containing nitrite reductase of *Achromobacter, cycloclastes,* J. Amer. Chem. Soc. 111 (1989) 2322-2323.

[19] M. Basaglia, A. Toffanin, E. Baldan, M. Bottegal, J. P. Shapleigh, S. Casella, Selenite-reducing capacity of the copper-containing nitrite reductase of *Rhizobium sullae*, FEMS Microbiol. Lett. 269 (2007)124–130.

[20] T. Kohzuma, M. Kikuchi, N. Horikoshi, S. Nagatomo, T. Kitagawa, R. S. Czernuszewcz, Intersite structural rearrangement by substrate binding: Spectroscopic studies of copper-containing nitrite reductase from *Alcaligenes xylosoxidans* NCIMB 11015, Inorg. Chem. 45 (2006) 8474-8476.

[21] M. Kukimoto, N. Nishiyama, M. E. P. Murphy, S. Turley, E. T. Adman, S. Horinouchi, T. Beppu, X-ray structure and site-directed mutagenesis of a copper nitrite reductase from *Alcaligenes faecalis* S-6, Biochemistry 33 (1994) 5246-5252.

[22] M. Fittipaldi, H. J. Wijma, M. P. Verbeet, G. W. Canters, E. J. J. Groenen, M. Huber, The substrate-bound Type 2 copper site of nitrite reductase: The nitrogen hyperfine coupling of nitrite revealed by pulsed EPR, Biochemistry 44 (2005) 15193-151202.

[23] M. Prudêncio, G. Sawers, S. A. Fairhurst, F. K. Yousafzai, R. R. Eady. *Alcaligenes xylosoxidans* Dissimilatory nitrite reductase: Alanine substitution of the surface-exposed histidine 139 ligand of the Type 1 Copper centre prevents electron transfer to the catalytic centre, Biochemistry 41 (2002) 3430-3438.

[24] H. J. Wijma, M. J. Boulanger, A. Molon, M. Fittipaldi, M. Huber, M. E. P. Murphy, M. P. Verbeet, G. W. Canters, Reconstitution of the Type-1 Active site of the H145G/A variants of nitrite reductase by ligand insertion, Biochemistry 42 (2003) 4075-4083.

[25] K. Sen, S. Horrell, D. Kekilli, C. W. Yong, T. W. Keal, H. Atskisi, D. W. Moreau, R. E. Thorne, M. A. Hough, R. W. Strange, Active site protein dynamics and solvent accessibility in native *Achromobacter cycloclastes* copper nitrite reductase, IUCrJ 4 (2017) 495-505.

[26] M. A. Hough, R. R. Eady, S. S. Hasnain, Identification of the proton channel to the active site type 2Cu centre of nitrite reductase: structural and enzymatic properties of the H254Phe and Asn90Ser mutants, Biochemistry, 47 (2008) 13547-13553.

[27] N. G. H. Leferinck, C. Han, S. V. Antonyuk, S. E. J. Rigby, M. A. Hough, R. R. Eady, N. S. Scrutton S. S. Hasnain, Mechanism of proton coupled electron transfer in the catalytic cycle of *Alcaligenes xylosoxidans* copper-dependent nitrite reductase, Biochemistry 50 (2011) 4121-4131.

[28] E.T. Adman, J. W. Godden, S. Turley, J. Biol. Chem. The structure of copper-nitrite reductase from *Achromobacter cycloclastes* at five pH values with NO_2^- bound and type ll copper deleted, 270 (1995) 27458-27474.

[29] E. I. Tocheva, F. I. Rosell, A. G. Mauk, M. E. P. Murphy, Side-on copper nitrosyl coordination by nitrite reductase, Science 304 (2004) 867-870.

[30] E. I. Tocheva, F. I. Rosell, A. G. Mauk, M. E. P. Murphy, Stable copper-nitrosyl formation by nitrite reductase in either oxidation state, Biochemistry, 46 (2007) 12366-12374.

[31] M. A. Hough, J. Conradie, R. W. Strange, S. V. Antonyuk, R. R. Eady, A. Ghosh, S. S. Hasnain, Nature of the copper-nitrosyl intermediates of copper nitrite reductases during catalysis, Chem. Sc. 11 (2020) 12485-12492.

[32] S. L. Rose, S. V. Antonyuk, D. Sasaki, K. Yamashita, K. Hirata, G. Ueno, R. R. Eady, T. Tosha, M. Yamamoto, S. S. Hasnain, An unprecedented insight into the catalytic mechanism of copper nitrate reductase from atomic-resolution and damage-free structures, Science Advances 7 (2021) eadb8523.

[33] S.Horrell, S. V. Antonyuk, R. R. Eady, S. S. Hasnain, M. A. Hough, R. W. Strange, Serial crystallography captures enzyme catalysis in copper nitrite reductase at atomic resolution from one crystal, IUCrJ 3 (2016) 271-281.

[34] H. J. Wijma, L. J. C. Jeuken, M. P. Verbeet, F. A. Armstrong, G. W. Canters, A random sequential mechanism for nitrite binding and active site reduction in copper nitrite reductase, J. Biol. Chem. 281 (2006) 16340-16346.

[35] L. Krzemiński, L. Ndamba, G. W. Canters, T. J. Aartsma, S. D. Evans, L. J. C. Jeuken, Spectroelectrochemical investigation of intramolecular and interfacial electron-transfer rates reveals differences between nitrite reductase at rest and during turnover, J. Amer. Chem. Soc. 133 (2011) 15085-15093.

[36] R. H. Goldsmith, L. C. Tabares, D. Kostrz, C. Dennison, T. J. Aartsma, G. W. Canters, W. E. Moerner, Redox cycling and kinetic analysis of single molecules of solution phase nitrite reductase, Proc. Natl. Acad. Sci. USA 108 (2011) 17269–17275.

[37] M. E. P. Murphy, S. Turley, E. T. Adman, Structure of nitrite bound to copper-containing nitrite reductase from *Acaligenes faecalis*: Mechanistic implications, J. Biol. Chem. 45 (1997) 28455-28460.

[38] R. W. Strange, L. M. Murphy, F. E. Dodd, Z. H. L. Abraham, R. R. Eady, B. E. Smith S. S. Hasnain, Structural and kinetic evidence for an ordered mechanism in copper nitrite reductase, J. Molec. Biol. 287 (1999) 1001-1009

[39] T. P. Halstead, K. Yamashita, C. C. Gopalasingsm, R. T. Shenoy, K. Hirata, H. Ago, G. Ueno, M. P. Blakeley, R. R. Eady, S. V. Antonyuk, M. Yamamoto, S. S. Hasnain, Catalytically important damage-free structures of a copper nitrite reductase obtained by femptosecond X-ray laser and room temperature neutron crystallography IUCrJ 6 (2019) 761-772.

[40] M. J. Hough, S. S. Hasnain, Structure of fully reduced bovine copper zinc superoxide dismutase at 1.15Å, Structure 11 (2003) 937-946.

[41] S. V. Antonyuk, C. Han, R. R. Eady, S. S. Hasnain, Structures of protein-protein complexes involved in electron transfer, Nature (Lond.) 496 (2013) 123-127.

[42] S. Ghosh, A. Dey, Y. Sun, C. P. Scholes, E. I. Solomon, Spectroscopic and computational studies on nitrite reductase: proton induced electron transfer and backbonding contributions to reactivity, J. Amer. Chem. Soc. 131 (2009) 277-288.

[43] Y. Fukuda, T. Inoue, High temperature and high-resolution crystallography of thermostable copper nitrite reductase, Chem. Comm. 51 (2015) 6532-6535.

[44] D. J. Opperman, D. H. Murgida, S. D. Dalosto, C.D. Brondino, F. M. Ferroni, A three domain copper-nitrite reductase with a unique sensing loop, IUCrJ 6 (2019) 248-258.

[45] M. J. Boulanger, M. E. P. Murphy, Directing the mode of nitrite binding to copper-containing nitrite reductase from *Alcaligenes faecalis* S-6 : Characterisation of an active site leucine, Prot. Sci 12 (2003) 248-256.

[46] Y Zhao, D. A. Lukoyanov, Y. V. Toropov, K. Wu, J. P. Shapleigh, C. P. Scholes, Catalytic function and local proton structure at the type 2 copper of nitrite reductase: The correlation of enzymatic pH dependence, conserved residues, and proton hyperfine structure, Biochemistry 41 (2002) 7464-7474.

[47] F. Jacobson, A. Pistorius, D. Farkas, W. DeGrip, Ö Hansson, L. Sjölin R. Neutze, pH dependence of copper geometry, reduction potential, and nitrite affinity in nitrite reductase, J. Biol. Chem. 282 (2007) 6347-6355.

[48] S. Ghosh, A. Dey, O. M. Usov, Y. Sun, V. M. Grigoryants, C. P. Scholes, E. I. Solomon, Resolution of the spectroscopy versus crystallography issue for NO intermediates of nitrite reductase of *Rhodobacter sphaeroides,* J. Am. Chem. Soc. 129 (2007) 10311-10310.

[49] D. Pinho, S. Besson, C. D. Brondino, B. deCastro, I. Moura, Copper-containing nitrite reductase from *Pseudomonas chloroaphis* DSM 50135: Evidence for modulation of the rate of electron transfer through nitrite binding to the type 2 copper centre, Eur. J. Biochem. 271 (2004) 2361-2369.

[50] F. K. Yousafzai, R. R. Eady, Dithionite reduction kinetics of the dissimilatory copper-containing nitrite reductase of *Alcaligenes xylosoxidans* : The SO_2^- radical binds to the substrate binding site before the type 2 copper is reduced, J. Biol. Chem. 37 (2002) 34067-34073.

[51] M. A. Hough, S. V. Antonyuk, R. R. Eady, S. S. Hasnain, Crystallography with on-line optical and X-ray absorption spectroscopy demonstrates an ordered mechanism in Cu-nitrite reductase, J. Molec. Biol. (2008) 738 353-361.

[52] R. G. Hadt, S. I. Gorelsky, E. I. Solomon, Anisotropic covalency contributions to super-exchange pathways in Type 1 copper sites J. Amer. Chem. Soc. 136 (20140 15034-15045.

[53] K. Kobayashi, Pulse radiolysis studies for mechanism in biochemical redox reactions, Chem. Rev. 119 (2019) 4413-4462.

[54] K. Kobayashi, S. Tagawa, Deligeer, S.Suzuki, The pH dependent changes of intramolecular electron transfer on copper-containing nitrite reductase, J. Biochem. 126 (1999) 408-412.

[55] O. Farver, R. R. Eady, I. Pecht, Reorganisational energies of the individual copper centres in dissimilatory nitrite reductases: Modulation and control of internal electron transfer, J. Phys. Chem. A 108 (2004) 9005-9007.

[56] H. T. M. Hedison, M. Shanmugam, D. J. Heyes, R. Edge, N. S. Scrutton, Active intermediates in copper nitrite reductase reactions probed by a cryotrapping paramagnetic resonance approach, Angewandte Chemie. 10.1002/anie.202005052.

[57] S. Brenner, D. J. Heyes, S. Hay, M. A. Hough, R. R. Eady, S. S. Hasnain, N. S. Scrutton, Demonstration of proton coupled electron transfer in the copper-containing nitrite reductases, J. Biol. Chem. 284 (2009) 25973-25983.

[58] H. T. M. Hedison, D. J. Heyes, M. Shaanmugam, A. I. Iorgu, N. S. Scrutton, Solvent slaved protein motions accompany proton coupled electron transfer reactions catalyzed by copper nitrite reductase, Chem. Comm. 55 (2019) 5863-5866.

[59] M. J. Ellis, S. G. Buffey, M. A. Hough, S. S. Hasnain, On-line optical and X-ray spectroscopies with crystallography: an integrated approach for determining metalloprotein structures in functionally well defined states, J. Synch. Rad. 15 (2008) 433-439.

[60] S. Suzuki, K. Kataoka, K. Yamaguchi, Metal coordination and mechanism of multicopper nitrite reductase, Acc. Chem. Res. 33 (2000) 728-735.

[61] N. G. H. Leferinck, S. V. Antonyuk, J. A. Houwman, N. S. Scrutton R. R. Eady, S. S. Hasnain, Impact of residues remote from the active centre on enzyme catalysis of copper nitrite reductase, Nature Comm. 5 (2014) 4395-4395.

[62] S. Ghosh, X. Xie, A. Dey, Y. Sun, C. P. Scholes, E. I. Solomon, Thermodynamic equilibrium between blue and green copper sites and the role of protein in controlling function, Proc. Natl. Acad. Sci. USA 106 (2009) 4969-4974.

[63] E. I. Solomon, R. K. Szilagyi, S. DeBeer Goerge, L. Basumallick, Electronic structures of metal sites in proteins and models: Contributions to function in blue copper proteins, Chem. Rev. 104 (2004) 419-458.

[64] A. Vaselov, K. Olesen, S. Sienkiewicz, J. P. Shapleigh, C. P. Scholes, Biochemistry 37 (1998) 6095-6105.

[65] L. C. Tabares, A. Gupta, T. J. Aartsma, G. W. Canters, Tracking electrons in biological macromolecules : from ensemble to single molecule, Molecules 19 (2014) 11660-11678.

[66] S Kuznetsova, G. Zauner, T. J. Aartsma, H. Engelkamp, N. Hatzakis, A. E. Rowan, R. J. M. Christianen, G. W. Canters, The enzyme mechanism of nitrite reductase studied at single molecular level, Proc. Natnl. Acad. Sci. USA 105 (2008) 3250-3255.

[67] L. C. Tabares, D. Kostrz, A. Elmalk, A. Andreoni, C. Dennison, T. J. Aartsma, G. W. Canters, Fluorescence lifetime analysis of nitrite reductase from *Alcaligenes xylosoxidans* at the single molecule level reveals the enzyme mechanism, Chem. Eur. J 17 (2011) 12015-12019.

[68] N. G. H. Leferinck, R. R. Eady, S. S. Hasnain, N. S. Scrutton, Laser-flash photolysis indicates that internal electron transfer is triggered by proton uptake by *Alcaligenes xylosoxidans* copper-dependent nitrite reductase, FEBS J. 279 (2021) 2174-2181.

[69] Y. Fukuda, K. M. Tse, M. Suzuki, K. Diederichs, K. Hirata, T. Nakane, M. Sugahara, E. Nango, K. Tono, Y. Joti, T. Kameshima, C. Song, T. Hatsui, M. Yabashi, O. Nureki, H. Matsumura, T. Inoue, S. Iwata, E. Mizohata, Redox-coupled structural changes in nitrite reductase revealed by serial femtosecond and microfocus crystallography, J. Biochem. 159 (2016) 527–538.

[70] Y. Fukuda, K. M. Tse, T. Nakane, T. Nakatsu, M. Suzuki, M. Sugahara, S. Inoue, T. Masuda, F. Yumoto, N. Matsugaki, E. Nango, K. Tono, Y. Joti, T. Kameshima, C. Song, T. Hatsui, M. Yabashi, O. Nureki, M. E. P. Murphy, T. Inoue, S. Iwata, E. Mizohata, Redox- coupled structural proton transfer mechanism in nitrite reductase revealed by femtosecond crystallography, Proc. Natl. Acad. Sci. USA 113 (2016) 2928-2933.

[71] T. P. Halstead, K. Yamashita, K. Hirata, H. Ago, G. Ueno, T. Tosa, , R. R. Eady, S. V. Antonyuk, M. Yamamoto, S. S. Hasnain, An unexpected dioxygen species revealed by serial femptosecond rotational crystallography in copper nitrite reductase, 5 IUCrJ (2018) 22-31.

[72] Y. Fukuda,T. M. Matsusaki, K. M. Tse, E. Minohata, M. E. P. Murphy, T. Inoue, Crystallographic study of dioxygen chemistry in a copper-containing nitrite reductase from *Geobacillus thermodenitrificans,* Acta Cryst. D 74 (2018) 769-777.

[73] Y. Fukuda, K. M. Tse, Y. Kado, E. Minohata, H. Matsumura, T. Inoue, Insights into unknown foreign ligand in copper nitrite reductase, Biochm. Biophys. Res. Comm. 464 (2015) 622-628.

[74] M. Nojiri, H. Koteishi, T. Nakagami, K. Kobayashi, T. Inoue, K. Yamaguchi, S. Suzuki, Structural basis of inter-protein electron transfer for nitrite reductase in denitrification, Nature, 642 (2009) 117-120.

[75] S. Horrell, K. Yamishita,C. C. Gopalasingam, R. J. Shenoy, K. Hirata, H. Ago, G. Ueno, M. P. Blakeley, R. R. Eady, S. V. Antonyuk, M. Yamamoto, S. S. Hasnain, Catalytically important damage-free structures of copper nitrite reductase obtained by femptosecond X-ray laser and room temperature neutron crystallography, IUCrJ 6 (2019) 761-772.

[76] S. Horrell, D. Kekilli, K. Sen, R. L. Owen, F. S. N. Dworsowski, S. V. Antonyuk, T. W. Keal, C. W. Yong, R. R. Eady, S. S. Hasnain, R. W. Strange, M. A. Hough, Enzyme catalysis captured using multiple structures from one crystal at varying temperatures, IUCrJ 5 (2018, 283-292.

[77] A. C. Merket, N. Lehnert, Binding and activation of nitrite and nitric oxide by copper nitrite reductase and corresponding model complexes, Dalton Trans. 41 (2012) 3355-3368.

[78] O. M. Usov, Y. Sun, V. M. Grigoryants, J. P. Shapleigh, C. P. Scholes, EPR-ENDOR of the Cu(I)NO complex of nitrite reductase, J. Amer. Chem. Soc. 128 (2006) 13102-13111.

[79] H. J. Wijma, G. W. Canters, S. de Vries, M. P. Verbeet, Bidirectional catalysis by copper-containing nitrite reductase, Biochemistry 43 (2004) 10467-10474.

[80] M. A. Jackson, J. M. Tiedje, B. A. Averill, Evidence for an NO-rebound mechanism for production of N_2O from nitrite by the copper containing nitrite reductase from *Achromobacter cycloclastes,* FEBS Lett. 291 (1991) 41-44.

[81] M. K, Kataoka, H. Furusawa, K. Takagi, K.Yamaguchi, S. Suzuki, Functional analysis of conserved aspartate and histidine residues located around the type 2 copper site of copper-containing nitrite reductase, J. Biochem. 127 (2000) 345-350.

[82] S. Suzuki, H. Furusawa, K. Katoka, K. Yamaguchi, M. Kobayashi, S. Tawaga, Intramolecular electron transfer in native and mutant forms of blue copper-containing nitrite reductase from *Alcaligenes xylosoxidans*, Inorg. reaction mechanisms 2 (2000) 129-135.

[83] M. J. Ellis, J. G. Grossman, R. R. Eady, S. S. Hasnain, Genomic analysis reveals widespread occurrence of new classes of copper nitrite reductase, J. Biol. Inorg. Chem. 12 (2005) 1119-1127.

[84] S. V., Antonyuk, R. R. Eady, S. S. Hasnain, Three-domain heme-c nitrite reductases, In encyclopeida of inorganic and bioinorganic chemistry 2001 John Wiley and son DOI:10.1002/9781119951438.cibc2316.

[85] M. Nojiri, Y. Xie, T. Inoue, T. Yamamoto, H. Matsumura, K. Kataoka, Deligeer, K. Yamaguchi, Y. Kai, S. Suzuki, Structure and function of a hexameric copper-containing nitrite reductase, Proc. Natl. Acad. Sci. USA 104 (2007) 4315-4320.

[86] D. Sasaki, T. F. Watanabe, R. R. Eady, R. C. Garratt, S. V. Antonyuk, S. S. Hasnain. Structures of substrate- and product-bound forms of a multidomain nitrite reductase shed light on the role of domain tethering in protein complexes, IUCrJ 7 (2020) 557-565.

[87] S. Suzuki, T. Maetani, M. Norjiri, K. Yamaguchi, M. Kobayashi, S. Tawaga Pulse radiolysis of hexameric nitrite reductase containing two type 1 Cu sites in a monomer, Bull.Chem. Soc. Jpn. 81 (2008) 1525-1527.

[88] Deligeer, R. Fukunaga, K. Kataoka, K.Yamaguchi, K. Kobayashi, S. Tagawa,

S. Suzuki Spectroscopic and functional organization of Cu-containing nitrite reductase from *Hyphomicrobium denitrificans,* J. Inorg. Biochem. 91 (2002) 132-138.

[89] Han, G. S. A. Wright, K. Fisher, S. E. J. Rigby, R. R. Eady, S. S. Hasnain, Characterisation of a novel copper heme *c* dissimilatory nitrite reductase from *Ralstonia picketti,* Biochem. J. 444 (2012) 219-226.

[90] J. Dong, D. Sasaki, R. R. Eady, S. S. Hasnain, (2018) Identification of a tyrosine switch in copper-heme nitrite reductases, 5 IUCrJ 510-518.

[91] A. Tsuda, R. Ishikawa, H. Koteishi, K. Tange, Y. Fukuda, K. Kobayashi, T. Inoue, M Norjiri, Structural and mechanistic insights into the electron flow through protein for cytochrome *c*-tethering copper nitrite reductase, J. Biochem. 154 (2013) 51-60.

[92] H. T. M. Hedison, R. T. Shenoy, A. I. Iorgu, D. J. Heyes, K. Fisher, G. Wright, S. Hay, R. R. Eady, S. V. Antonyuk, S. S. Hasnain, Unexpected role of a tether harbouring a tyrosine gatekeeper residue in modular nitrite reductase catalysis, ACS Catal. 9 (2019) 6087-6099.

[93] K. Sen, M. A. Hough, R. W. Strange, C. W. Yong, T. W. Keal, A QM/MM study of nitrite binding modes in a three-domain Heme-Cu Nitrite reductase, Molecules 23 (2018) 2997-3013.

[94] P. Mehrabi, R. Bücker, G. Bourenkov, H. M. Ginn, D. von Stetten, H. M. Müller-Werkmeister, T. Morizumi, B. T. Eger, W.-L. Ou, S. Oghbaey A. Sarracini, J. E. Besaw, O. Paré-Labosse, S. Meier, H. Schikora, F. Tellkamp,A. Marx, D. A. Sherrell, D. Axford, R. Owen, O. P. Ernst, E. F. Pai, E. C. Shultz, R. J. D. Miller, Serial femtosecond and serial synchrotron crystallography can yield data of equivalent quality: A systematic comparison, Sci. Adv. 7 (2021) : eabf1380 17 March 2021.

[95]. J. R. Stagno, Y. Lie, Y. R. Bhandari, C. E. Conrad, S. Panja,Structures of riboswitch RNA reaction states by mix-and-inject XFEL serial crystallography, Nature 541 (2017) 242-246.

Figure Captions.

Figure 1. Roles for CuNiR in the nitrogen cycle

Their involvement in denitrification, the stepwise reduction of nitrate to dinitrogen is a major well-studied role. Nitrification, the aerobic conversion of NH_3 to nitrite, and anammox, the anaerobic oxidation of NH_3 to N_2 using nitrite as electron acceptor are additional steps in which CuNiRs play a part.

Figure 2. Schematic representations of prototypic CuNiRs (*Ac*NiR/*Ax*NiR) with recently discovered N-terminal and C-terminal tethered three and four domain CuNiR where the core domains of prototypic CuNiRs is retained with widely different catalytic properties. Representative structures for each of these classes are shown in the lower half. The structure of a 4-domain CuNiR has yet to be determined.

Figure 3. Atomic resolution structure of Br^{2D}NiR showing the trimeric arrangement where each of the monomer (indicated by different colours) is comprised of two domains with T1Cu and T2Cu directly linked via a Cys-His bridge (indicated by yellow arrow showing hard-wired arrangement of a circuit) and the two sensor loops (indicated by the red arrows) reporting the status of T2Cu to T1Cu through subtle structural changes at the T2Cu site.

Figure 4. T2Cu site Br^{2D}NiR with nitrite bound and chemically generated NO. The nitrite bound structure is a XFEL FRIC structure at 1.3 Å resolution, showing single nitrite in side-on position and Asp92 in proximal conformation. The structure of NO-bound/T1Cu-reduced Br^{2D}NiR is at 1.19Å resolution shows a side-on NO position with slightly asymmetric distances of 2.17(4) and 2.08(3) Å for Cu–N and Cu–O, respectively.

Figure 5. Optical spectrum of a single crystal of Br^{2D}NiR showing T1Cu in the Cu^{2+} state while observing a well-defined LMCT charge transfer band at ~360 nm from nitrite to T2Cu in the nitrite-soaked crystals. Three conformations were observed for nitrite in high-resolution structures. The SRX structures showed T2Cu site with bidentate-bonded top-hat nitrite and “bent top-hat” conformation of nitrite. XFEL FRIC structure showed a single horizontal side-on coordination of nitrite.

Figure 6. Dose-dependent x-ray induced photo-reduction of a static *Ax*NiR crystal (A) spectra collected at 30 sec intervals showing the progressive reduction in the height of the 595 nm peak associated with conversion of $T1Cu^{2+}$ to $T1Cu^{+}$. The first twenty spectra and the final spectrum are plotted. (B) the dependence of the 595 nm peak height on absorbed x-ray dose. The time points indicative of MX and XAS data collection are shown. MX1 is time taken to complete first full crystallographic data set. (C). XAS spectra from the *Ax*NiR crystal following the collection of structures MX2 (solid line) and MX3 (dotted line). The spectra are consistent with a T2Cu in Cu^{2+} oxidation state in both cases. Inset - comparison of the edge region for oxidised and fully reduced *Ax*NiR crystals. In the reduced spectrum the 8984eV shoulder arising from T2Cu in Cu^{+} oxidation state is apparent.

Figure 7. The pH dependence profile of k_{CAT} and Inter–Cu k_{ET} of the prototypic *Ax*NiR with the N-terminal cupredoxin extended $Hd_{A3151}NiR$. Solid markers are the rate of Inter-Cu ET and open makers are *k*cat. The absence of a bell-shaped profile that characterises prototypic CuNiRs, attributed to the involvement of

Asp_{CAT} and His_{CAT}, is clear. AxNiR data adapted with permission from S. Suzuki, et, al. Acc. Chem. Res. 33 (2000) 728-735. Copyright 2000 Amer. Chem. Soc. (*Hd*$_{A3151}$*NiR* data adapted with permission from ref [88]. Copyright Elsevier (2002)

Figure 8. Scheme for alternate ordered-routes for nitrite reduction by prototypic CuNiR. Boxed species have been structurally characterised using EXFEL-FRIC on *Ac*NiR and *Br*^{2D}NiR (shown in blue). The scheme is based on kinetic data for prototypic CuNiRs where nitrite has been shown capable of binding to the T2Cu in both oxidation states, and on SRX structural movies of *Ax*NiR and *Ac*NiR during catalysis on route A. The relative flux through the two routes depends on pH and [nitrite].

Figure 9. The hexameric structure of *Hd*$_{1NES1}$NiR. The trimeric assembly from which hexamer is made is also shown below. Details of T1Cu of the additional domain and T1Cu/T2Cu of the core are given for *Hd*$_{1NES1}$NiR with residue numbering for *Hd*$_{A3151}$NiR. The NO_2^- is bound to the T2Cu in a side-on conformation via a single nitrogen atom and a single proximal oxygen atom with distances of 1.9 and 2.0 Å, respectively.

Figure 10. Comparison of experimental SAXS data with that calculated for a model, shown as inset, of *Rp*NiR created using the linker conformation of the RpNiR-core structure and refining the position of conformationally plastic cyt c domain, $\chi^2 = 1.5$. Lower panel shows a comparison of SAXS distance distribution functions (P(R)) for compact and elongated RpNiR.

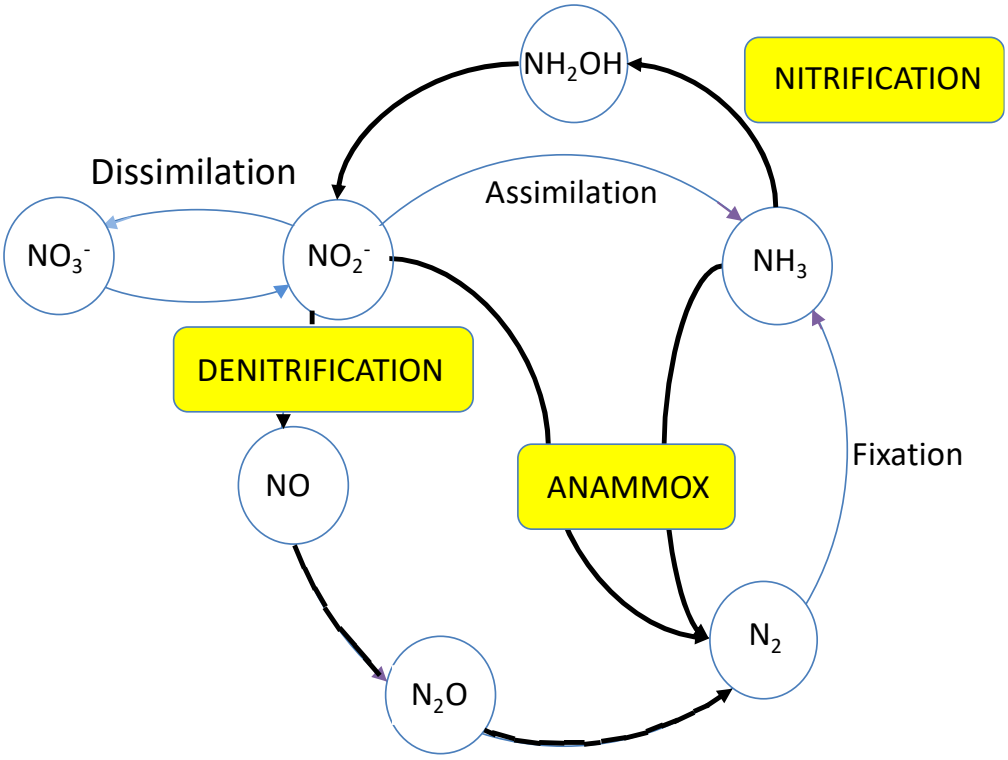
NH2OH
NITRIFICATION
Dissimilation
Assimilation
NO3-
NO2-
NH3
DENITRIFICATION
NO
ANAMMOX
Fixation
N2
N2O

Figure 1.

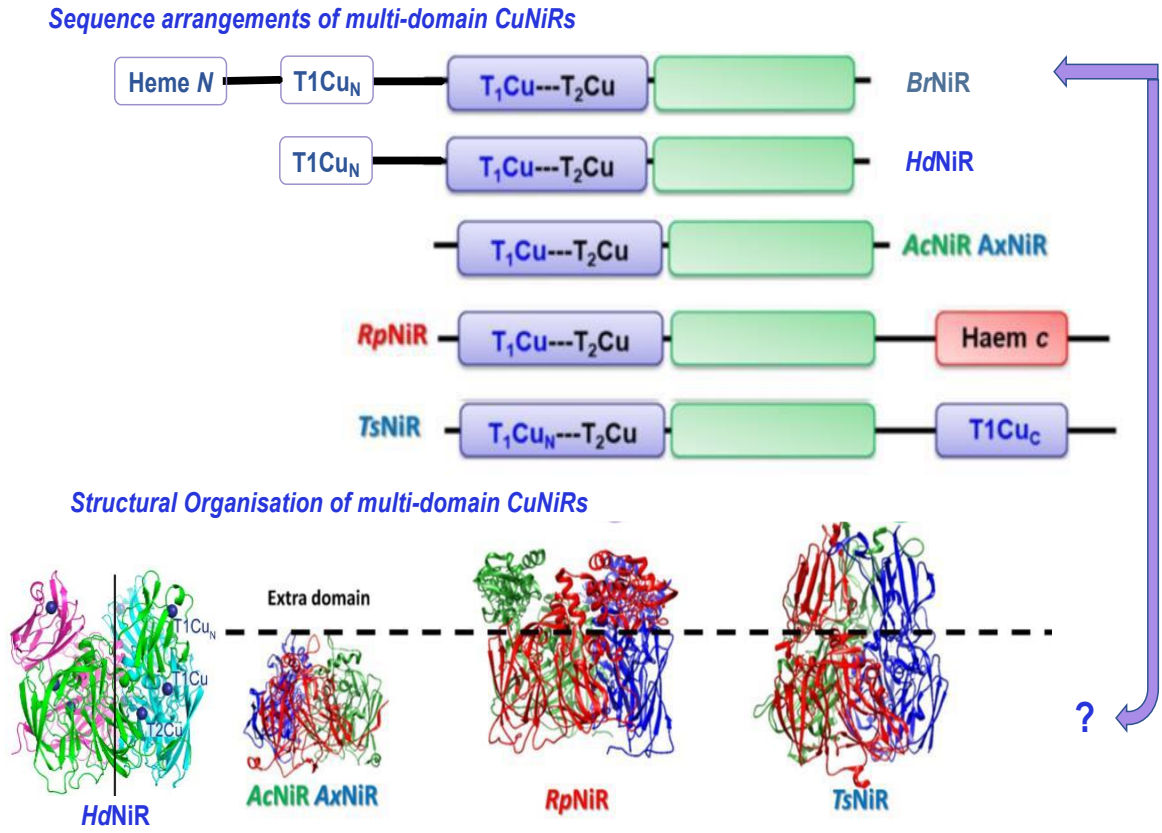

Figure 2

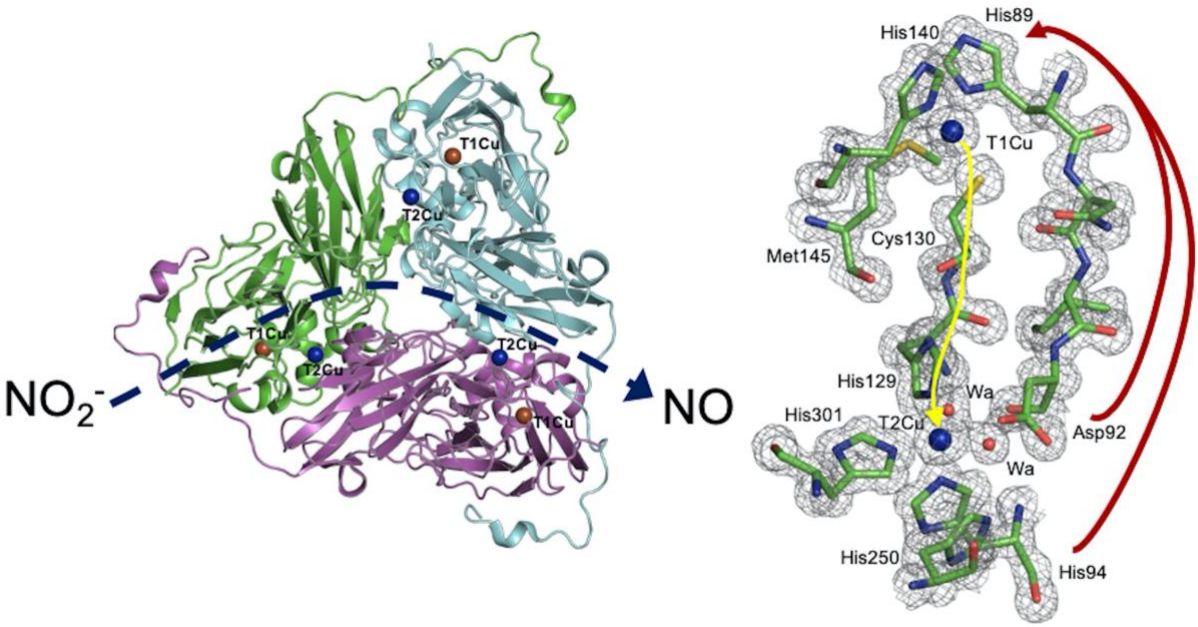

Figure 3

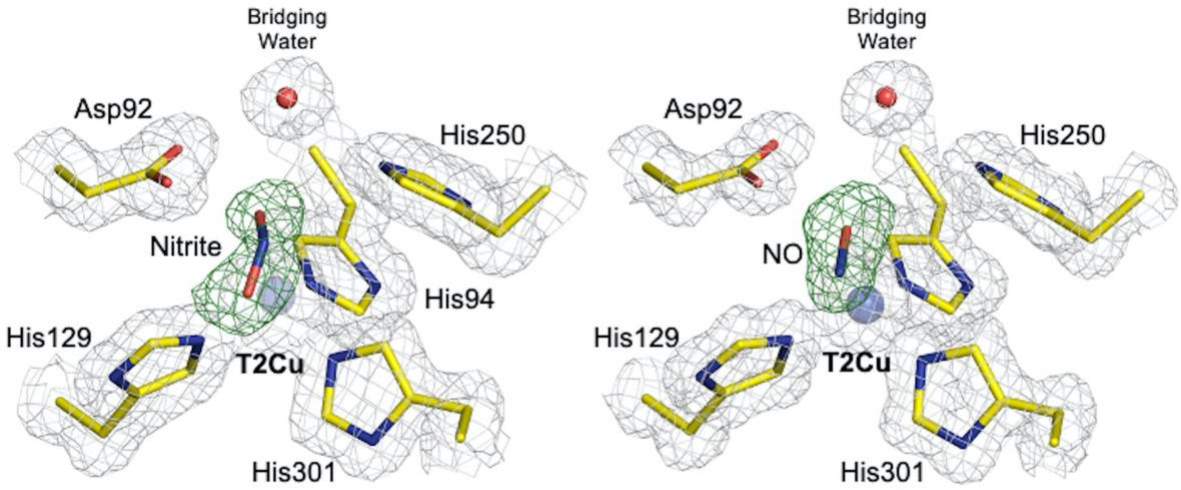

Figure 4

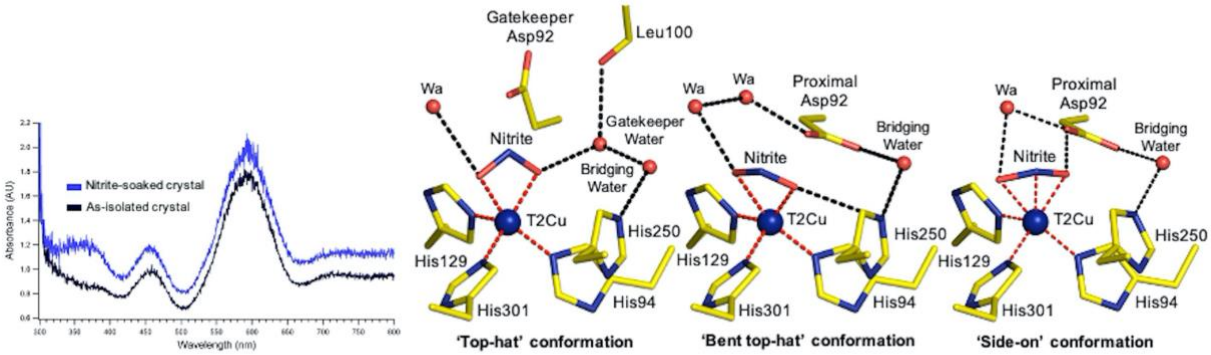

Figure 5

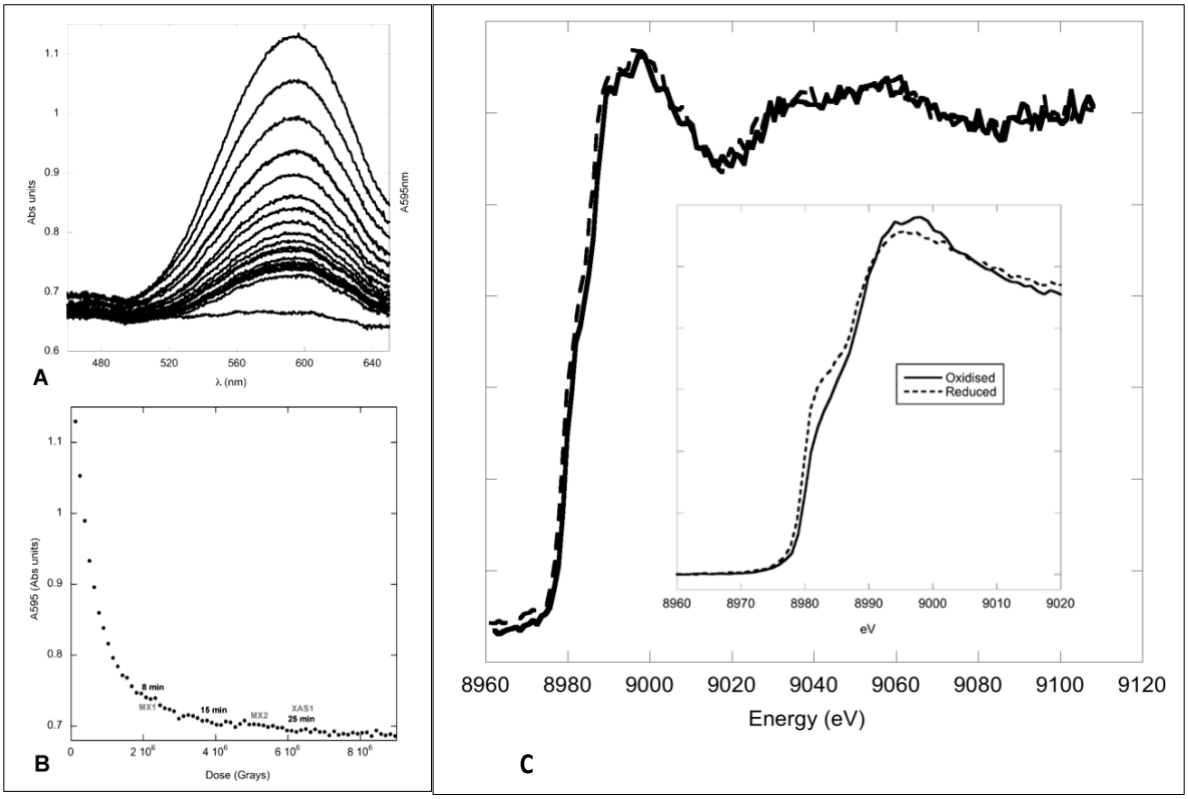
A
Abs units
A595nm
λ (nm)
B
A595 (Abs units)
Dose (Grays)
8 min
15 min
25 min
MX1
MX2
XAS1
C
Oxidised
Reduced
eV
Energy (eV)

Figure 6

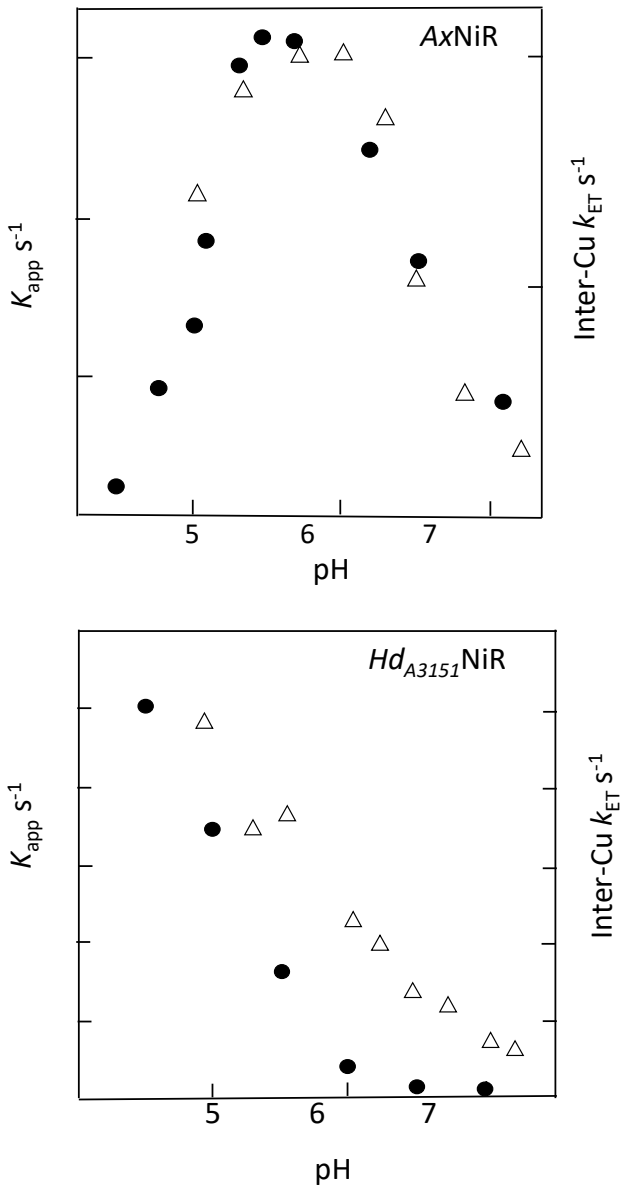
AxNiR
K_{app} s^{-1}
Inter-Cu k_{ET} s^{-1}
5
6
7
pH
Hd_{A3151}NiR
K_{app} s^{-1}
Inter-Cu k_{ET} s^{-1}
5
6
7
pH

Figure7

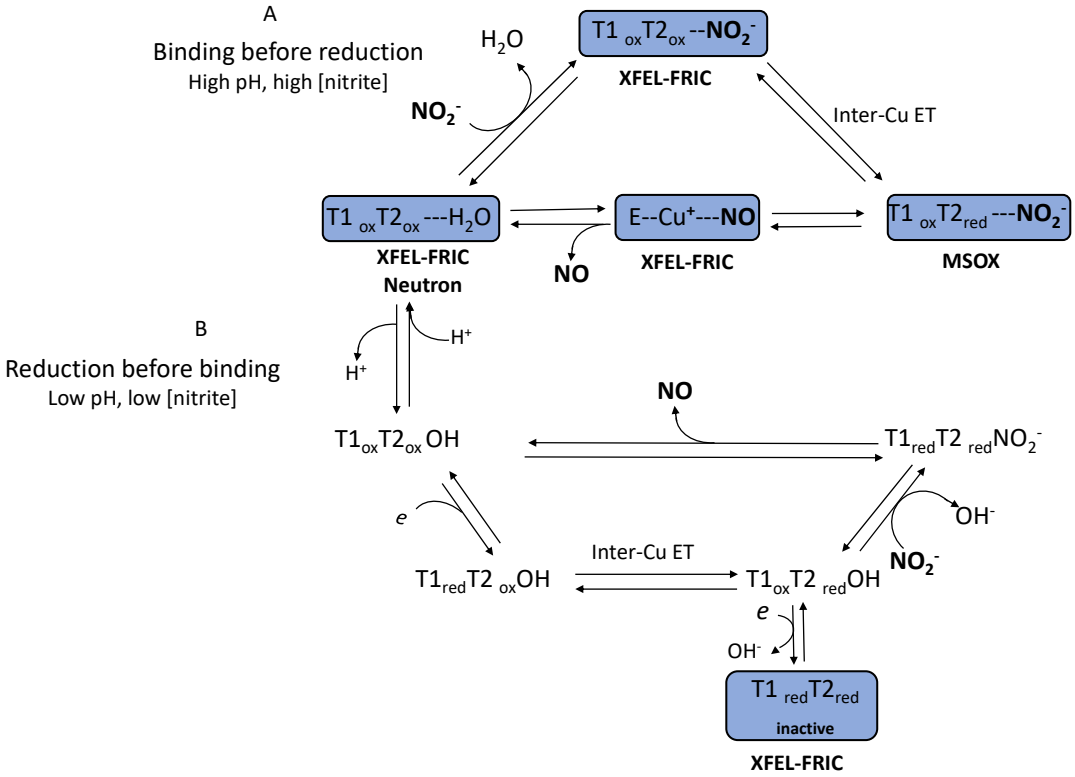
A
Binding before reduction
High pH, high [nitrite]
H_2O
NO_2^-
T1 $_{ox}$T2$_{ox}$--NO_2^-
XFEL-FRIC
Inter-Cu ET
T1 $_{ox}$T2$_{ox}$---H_2O
XFEL-FRIC
Neutron
E--Cu^+---NO
XFEL-FRIC
NO
T1 $_{ox}$T2$_{red}$ ---NO_2^-
MSOX
B
Reduction before binding
Low pH, low [nitrite]
H^+
H^+
NO
$T1_{ox}T2_{ox}$ OH
$T1_{red}T2_{red}NO_2^-$
e
OH^-
NO_2^-
Inter-Cu ET
$T1_{red}T2_{ox}OH$
$T1_{ox}T2_{red}OH$
e
OH^-
T1 $_{red}$T2$_{red}$
inactive
XFEL-FRIC

Figure 8.

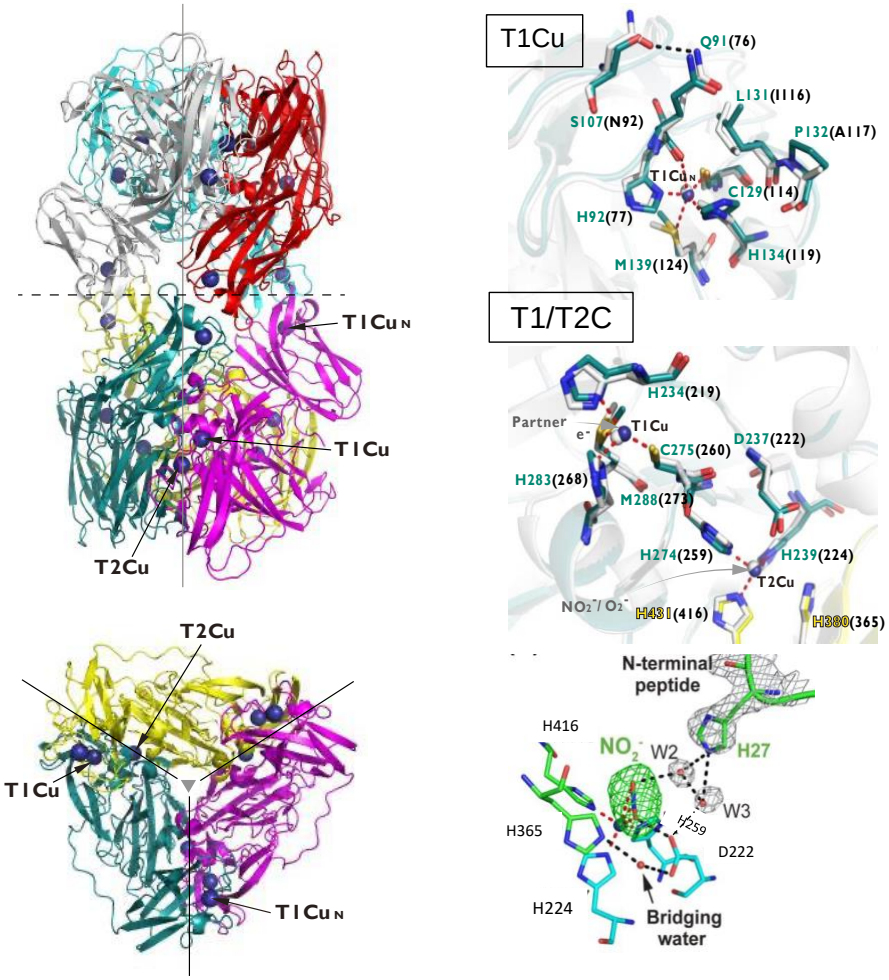
T1Cu
Q91(76)
L131(I116)
S107(N92)
P132(A117)
T1CuN
C129(114)
H92(77)
H134(119)
M139(124)
T1/T2C
H234(219)
Partner
e-
T1Cu
C275(260)
D237(222)
H283(268)
M288(273)
H274(259)
H239(224)
T2Cu
NO2-/O2
H431(416)
H390(365)
T1CuN
T2Cu
T2Cu
T1Cu
T1CuN
N-terminal peptide
H416
NO2-
W2
H27
W3
H365
H259
D222
H224
Bridging water

Figure 9

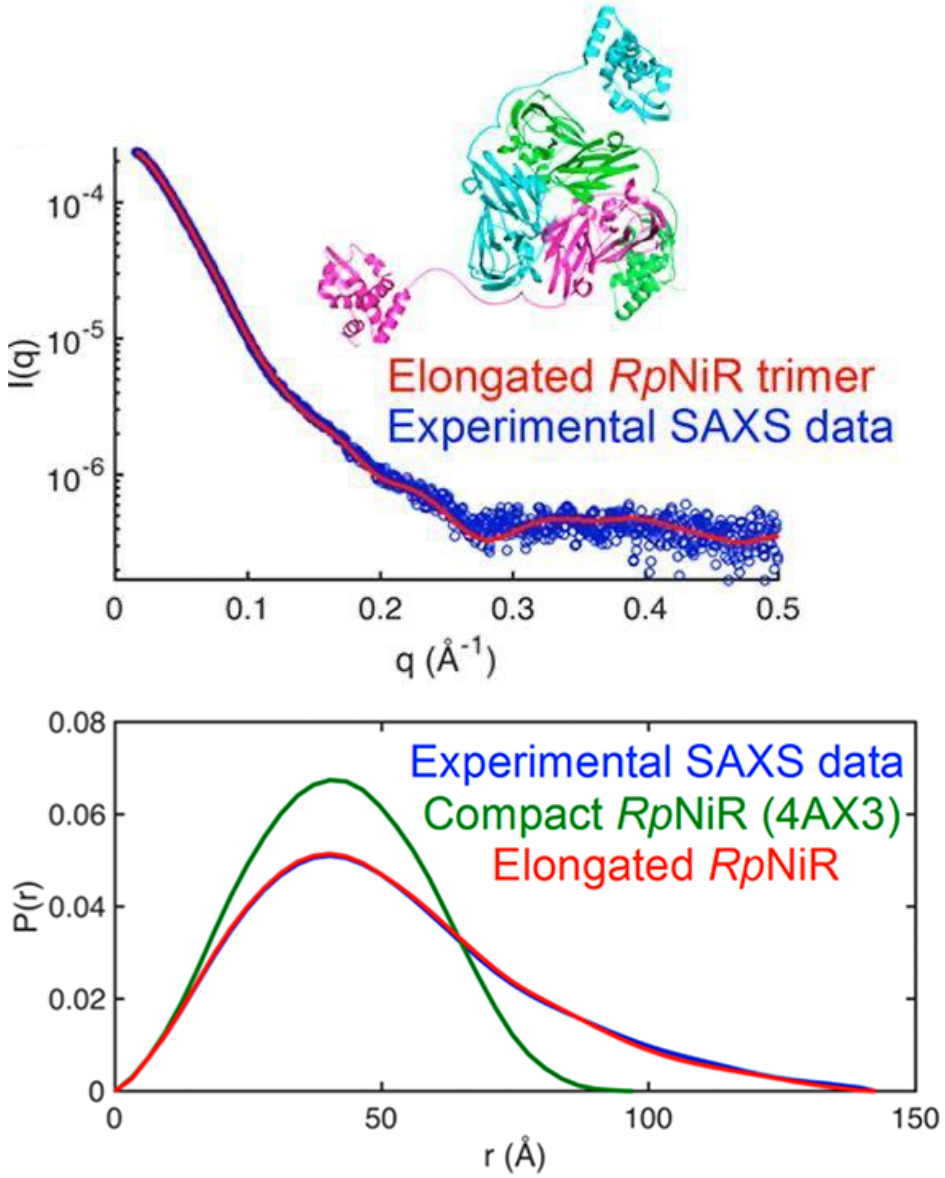
Elongated RpNiR trimer
Experimental SAXS data
I(q)
q (Å-1)
Experimental SAXS data
Compact RpNiR (4AX3)
Elongated RpNiR
P(r)
r (Å)

Figure 10